Acta Pharmaceutica Sinica B 2025;15(1):256–277

Chinese Pharmaceutical Association
Institute of Materia Medica, Chinese Academy of Medical Sciences

Acta Pharmaceutica Sinica B

www.elsevier.com/locate/apsb
www.sciencedirect.com

ORIGINAL ARTICLE

Reversing metabolic reprogramming by CPT1 inhibition with etomoxir promotes cardiomyocyte proliferation and heart regeneration *via* DUSP1 ADP-ribosylation-mediated p38 MAPK phosphorylation

Luxun Tang[a,b,c,†], Yu Shi[a,b,†], Qiao Liao[a,b,†], Feng Wang[a,b], Hao Wu[a,b], Hongmei Ren[a,b], Xuemei Wang[a,b], Wenbin Fu[a,b], Jialing Shou[a,b], Wei Eric Wang[a,b], Pedro A. Jose[d], Yongjian Yang[c,*], Chunyu Zeng[a,b,e,f,g,*]

[a]*Department of Cardiology, Daping Hospital, the Third Military Medical University (Army Medical University), Chongqing 400042, China*
[b]*Key Laboratory of Geriatric Cardiovascular and Cerebrovascular Disease Research, Ministry of Education of China, Chongqing Key Laboratory for Hypertension Research, Chongqing Cardiovascular Clinical Research Center, Chongqing Institute of Cardiology, Chongqing 400042, China*
[c]*Department of Cardiovascular Medicine, the General Hospital of Western Theater Command, Chengdu 610083, China*
[d]*Division of Renal Diseases and Hypertension, the George Washington University School of Medicine and Health Sciences, Washington, DC 20541, USA*
[e]*State Key Laboratory of Trauma, Burns and Combined Injury, Daping Hospital, the Third Military Medical University, Chongqing 400042, China*
[f]*Cardiovascular Research Center of Chongqing College, Chinese Academy of Sciences, University of Chinese Academy of Sciences, Chongqing 400042, China*
[g]*Department of Cardiology, the First Affiliated Hospital of Kunming Medical University, Kunming 650000, China*

Received 25 April 2024; received in revised form 22 June 2024; accepted 26 July 2024

*Corresponding authors.
E-mail addresses: chunyuzeng01@163.com (Chunyu Zeng), yangyongjian38@sina.com (Yongjian Yang).
[†]These authors made equal contributions to this work.
Peer review under the responsibility of Chinese Pharmaceutical Association and Institute of Materia Medica, Chinese Academy of Medical Sciences.

https://doi.org/10.1016/j.apsb.2024.11.001

KEY WORDS

Metabolic reprogramming;
Cardiomyocyte proliferation;
Carnitine palmitoyltransferase 1;
Etomoxir;
Fatty acid oxidation;
Glycolysis;
ADP-ribosylation;
p38 MAPK

Abstract The neonatal mammalian heart has a remarkable regenerative capacity, while the adult heart has difficulty to regenerate. A metabolic reprogramming from glycolysis to fatty acid oxidation occurs along with the loss of cardiomyocyte proliferative capacity shortly after birth. In this study, we sought to determine if and how metabolic reprogramming regulates cardiomyocyte proliferation. Reversing metabolic reprogramming by carnitine palmitoyltransferase 1 (CPT1) inhibition, using cardiac-specific *Cpt1a* and *Cpt1b* knockout mice promoted cardiomyocyte proliferation and improved cardiac function post-myocardial infarction. The inhibition of CPT1 is of pharmacological significance because those protective effects were replicated by etomoxir, a CPT1 inhibitor. CPT1 inhibition, by decreasing poly(ADP-ribose) polymerase 1 expression, reduced ADP-ribosylation of dual-specificity phosphatase 1 in cardiomyocytes, leading to decreased p38 MAPK phosphorylation, and stimulation of cardiomyocyte proliferation. Our present study indicates that reversing metabolic reprogramming is an effective strategy to stimulate adult cardiomyocyte proliferation. CPT1 is a potential therapeutic target for promoting heart regeneration and myocardial infarction treatment.

1. Introduction

Myocardial infarction (MI) and heart failure are the leading causes of death worldwide. The major cause of the pathological process is the loss of functional cardiomyocytes[1]. The adult mammalian heart is incapable of useful functional recovery following MI. However, studies have shown that modest cardiomyocyte turnover occurs in both physiological and pathological conditions, that is mediated primarily by the proliferation of pre-existing cardiomyocytes[2]. Although adult cardiomyocytes can reenter the cell cycle and form new cardiomyocytes after MI, the rate of cardiomyocyte proliferation *in vivo* is rather low. Therefore, the stimulation of adult cardiomyocyte proliferation becomes the key to cardiac regeneration[3].

It is known that metabolic reprogramming from fatty acid oxidation (FAO) to glycolysis triggers cell proliferation, as shown in cancer cells and somatic cells[4,5]. Interestingly, mammalian cardiomyocytes lose their proliferative capacity during early postnatal life (first week in rodent and porcine hearts)[2], which shares the same time-window with the conversion of perinatal cardiac energy metabolism from glycolysis to FAO[6]. It raises the question whether metabolic reprogramming is a secondary effect or a primary cause of cardiomyocyte proliferation. Several metabolic molecules were recently reported as regulators of the cardiomyocyte cell cycle. Inhibition of fatty acid β-oxidation metabolism delays cardiomyocyte cell cycle exit in the infant mouse heart[7]. Pyruvate kinase muscle isoenzyme 2 promotes cardiomyocyte proliferation, partially through redirecting glucose carbon flow into the anabolic pentose phosphate pathway, thereby reducing reactive oxygen species (ROS) production and DNA damage[8]. Inhibition of FAO by deleting *Cpt1b* promoted cardiomyocyte proliferation in adult mice and induced heart regeneration after ischemia-reperfusion injury[9]. These findings indicate that metabolic enzymes influencing glycolysis and/or FAO could regulate cardiomyocyte proliferation. Our present study indicated the effect of FAO inhibition on cardiomyocyte regeneration, and showed the translational significance by using CPT1 inhibitor (etomoxir), moreover, we investigated the novel mechanisms underlying the proliferative effect by FAO inhibition after MI.

2. Materials and methods

2.1. Animal models

Neonatal (P7) C57BL/6J mice were used in the experiments. Etomoxir (ETX, 20 mg/kg, MedChemExpress, Princeton, NJ, USA) was intraperitoneally injected daily from Day 7 to Day 14.

Adult C57BL/6J mice were subjected to MI by ligation of the proximal aspect of the left anterior descending (LAD) coronary artery. Surgeries were performed as described[10]. In brief, 8-week-old mice were anesthetized with 5% isoflurane/95% oxygen in an airtight chamber and placed in a supine position on a heating pad (37 °C). Following tracheal intubation, the mice were artificially ventilated using a volume-controlled ventilator with 2.4% isoflurane/97.6% oxygen. Following depilation and skin incision, lateral thoracotomy at the third intercostal space was performed by blunt dissection of the intercostal muscles. The LAD coronary artery was ligated using a 7-0 prolene suture. Subsequently, the thoracic wall incisions were sutured with 6.0 non-absorbable silk sutures, and the wounds were closed using skin adhesive, Vetbond (3M, MN, USA). The mice were then warmed for several minutes until recovery. After the surgery, ETX (20 mg/kg) was intraperitoneally injected daily for 2 weeks, according to previous studies[11,12]. Immunostaining for cardiomyocyte proliferation was performed 2 weeks post-MI and echocardiography was performed 4 weeks post-MI. All experiments were performed on age- and sex-matched mice, and the results show the female and male data together in the same graph. All experiments were approved by the Laboratory Animal Welfare and Ethics Committee of the Army Medical University (No. AMUWEC2017109).

2.2. Histology

Mouse hearts were harvested and fixed in 4% paraformaldehyde (PFA, Sangon Biotech, Shanghai, China)/phosphate-buffered saline (PBS) solution overnight at room temperature and then processed for paraffin sectioning. For analysis of cardiac regeneration following MI or drug injection, paraffin sections were serially cut at 0.5 mm intervals throughout the entire ventricle from the apex to the base. Masson's trichrome staining was

performed according to standard procedures. Scar size was quantified by ImageJ software, based on Masson's trichrome staining. Scar size was calculated relative to left ventricle size.

2.3. Immunofluorescence analysis

The heart sections were blocked with 5% bovine serum albumin (BSA) in PBS containing 0.1% Triton X-100 for 1 h at room temperature after antigen retrieval with 1 mmol/L ethylene diamine tetraacetic acid (EDTA) in boiling water for 20 min. Adherent cells were washed twice with PBS and then fixed in 4% PFA/PBS solution for 15 min. The fixed cells were washed three times with PBS, permeabilized with 0.1% Triton X-100 in PBS for 15 min, and then blocked with PBS containing 0.1% Triton and 3% BSA for 30 min at room temperature. Then, the cardiomyocytes or heart sections were incubated with primary antibodies overnight at 4 °C. The cardiomyocytes or heart sections were subsequently washed 3 times with PBS and incubated with corresponding secondary antibodies conjugated to Alexa Fluor 488 or 555 or 647 (Thermo Fisher Scientific, Waltham, MA, USA) for 2 h at 37 °C. The slides were mounted in antifade mounting medium. Primary antibodies used are following: anti-sarcomeric α-actinin antibody (Sigma−Aldrich, Darmstadt, Germany; Mouse, 1:100), anti-Ki67 antibody (Cell Signaling Technology, Danvers, MA, USA; Rabbit, 1:100), anti-phospho histone H3 Ser10 (PH3) antibody (Cell Signaling Technology; Rabbit, 1:100), anti-tropomyosin antibody (Sigma; Mouse, 1:100), anti-cardiac troponin T antibody (Thermo Fisher Scientific; Mouse, 1:100), anti-green fluorescent protein (GFP) antibody (Abcam, Cambridge, UK; Goat, 1:100), and anti-red fluorescent protein (RFP) antibody (Rockland Immunochemicals, Limerick, PA, USA; Rabbit, 1:100). 4,6-Diamidino-2-phenylindole dihydrochloride (DAPI, Solarbio, Beijing, China) was used for nuclear staining. To detect apoptosis of cardiomyocytes, sections were processed using an In Situ Cell Death Detection Kit (Roche, Shanghai, China). For the quantification of the number of Ki67 positive ($Ki67^+$) or PH3 positive ($PH3^+$) cardiomyocytes, the results acquired from sections of the heart harvested from each animal with at least 5 different fields and positions for each section were averaged. To calculate the rate of proliferating cardiomyocytes, we counted the total number of cardiomyocyte nuclei per field. To calculate the total number of cardiomyocytes in each culture plate, 10 random fields were selected, and the total number of cardiomyocytes was estimated. The total number of cardiomyocytes in the culture plate was estimated by Eq. (1):

$$\text{The total number of cardiomyocytes} = \text{The average number of cardiomyocytes in each field} \times \text{The area of the culture plate} / \text{The area of each field} \quad (1)$$

To calculate the rate of proliferating cardiomyocytes in mosaic analysis with double markers mice, we counted the total labeled and single-color cardiomyocytes per field. To calculate the rate of proliferating cardiomyocytes *in vitro*, we counted the total number of cardiomyocytes and the number of $Ki67^+$ or $PH3^+$ cardiomyocytes in at least 10 different fields and positions captured for each group. In all cell counting experiments, the fields of view were randomized to reduce counting bias.

After antigen retrieval with 1 mmol/L EDTA in boiling water for 20 min, the heart sections were washed three times with PBS, and then permeabilized with 0.1% Triton X-100. After washing with PBS three times, the sections were incubated with wheat germ agglutinin (WGA) conjugated to Alexa Fluor 488 (50 mg/mL, Thermo Fisher Scientific) for 30 min at room temperature. The border zone was defined as the 2 mm area encircling the area of infarction[13]. To quantify the cell size, 5 different fields and positions per sample were captured at 40 × magnification. ImageJ software was used to quantify the size of each cell.

2.4. Echocardiography

Mice were anesthetized with 3% isoflurane induction following maintenance at 1%−2% by nose cone. Heart function was evaluated by transthoracic echocardiography, using a Vivid E9 device (General Electric Company). All echocardiography measurements were performed in a blind manner.

2.5. mRNA microarray analysis

Total RNA was extracted from postnatal Day 14 (P14) heart tissue after treatment with vehicle (saline) or ETX for 1 week. All samples were acquired in three replicates for mRNA microarray analysis. Using the Ambion® Whole Transcript Expression Kit (Affymetrix, Thermo Fisher Scientific), the total RNA (20−50 ng) was reverse-transcribed to synthesize first-strand cDNA containing a T7 promoter sequence. DNA polymerase and RNase H were used to degrade the RNA and synthesize second-strand cDNA, simultaneously. Then, antisense cRNA was synthesized and amplified by *in vitro* transcription of the second-strand cDNA template using T7 RNA polymerase. Enzymes, salts, inorganic phosphates, and unincorporated nucleotides were removed to improve the stability of the cRNA. The concentration of a cRNA solution was determined by measuring its absorbance at 260 nm, using a NanoDrop® Spectrophotometer (Thermo Fisher Scientific). The sense-strand cDNA, containing dUTP at a fixed ratio relative to dTTP, was synthesized by the reverse transcription of cRNA, using random primers. The cRNA template was degraded by RNase H leaving single-stranded cDNA. Enzymes, salts, and unincorporated dNTPs were removed to purify the second-strand cDNA. The concentration of a second-strand cDNA solution was determined by measuring its absorbance at 260 nm, using a NanoDrop® Spectrophotometer. The GeneChip® Whole Transcript Terminal Labeling Kit (Affymetrix) was used for the fragmentation and labeling of the cDNA. The hybridizations for cartridge arrays were set up using GeneChip® Hybridization, Wash, and Stain Kit (Affymetrix). Finally, the probe arrays were washed, stained, and scanned to generate the data.

2.6. Quantitative real-time PCR

The total RNA was extracted from P14 heart tissue or primary cardiomyocytes isolated from P1 or P7 rats after treatment with or without ETX. cDNA was synthesized by using the PrimeScript™ RT Master Mix (Takara Biomedical Technology, Beijing, China), according to the manufacturer's protocol. Quantitative real-time PCR was performed using SYBR® Premix Ex Taq™ II (Takara Biomedical Technology) on Real-Time PCR system (Bio-Rad Laboratories, Hercules, CA, USA). Values for specific genes were normalized to α-actin gene expression.

2.7. Western blot analysis

Total protein was extracted from P14 heart tissue or primary cardiomyocytes isolated from P1 or P7 rats after treatment with or without ETX. These proteins, which contained 50 μg of protein per sample, were separated by SDS-PAGE and electrophoretically transferred onto nitrocellulose membranes (Bio-Rad). After treatment with blocking buffer (Tris-buffered saline with 0.1% Tween® 20 detergent, TBST, with 5% BSA) at room temperature for 30 min, the membranes were probed with the primary antibodies at 4 °C overnight. The membranes were washed in TBST and incubated with the appropriate secondary antibodies (Li-Cor, IRDye® 800CW Goat anti-Rabbit, or IRDye® 800CW goat anti-mouse, 1:10,000) for 2 h at room temperature. The membranes were washed and visualized with an Odyssey Imaging System. PageRuler™ Plus (Thermo Fisher Scientific) and Page Ruler™ Unstained Protein Ladder (Thermo Fisher Scientific) were used as the protein ladders.

The primary antibodies were: anti-phospho p38 mitogen-activated protein kinase (p-p38 MAPK) alpha Thr180/Tyr182 antibody (Thermo Fisher Scientific; 36-8500, Rabbit, 1:500), anti-p38 MAPK antibody (Cell Signaling Technology; 9212, Rabbit, 1:1000), anti-dual-specificity phosphatases 1 (DUSP1) antibody (Cell Signaling Technology; 48625, Rabbit, 1:1000), anti-dual-specificity phosphatases 4 (DUSP4) antibody (Cell Signaling Technology; 5149, Rabbit, 1:1000), anti-dual-specificity phosphatases 12 (DUSP12) antibody (Proteintech, Wuhan, China; 67101-1-Ig, Mouse, 1:1000), anti-Poly/Mono-ADP ribose antibody (Cell Signaling Technology; 83732, Rabbit, 1:1000), anti-poly(ADP-ribose) polymerase family, member 1 (PARP1) antibody (Proteintech; 66520-1-Ig, Mouse, 1:1000), anti-mitogen-activated protein kinase 3 (MAP2K3) antibody (Proteintech; 80137-1-RR, Rabbit, 1:1000), anti-CPT1A antibody (Abcam; ab234111, Rabbit, 1:1000), anti-CPT1B antibody (Proteintech; 22170-1-AP, Rabbit, 1:1000), and anti-glucokinase (GCK) antibody (Proteintech; 19666-1-AP, Rabbit, 1:1000). Anti-β-actin (Proteintech; 66009-1-Ig, Mouse, 1:2000) was used for the normalization of protein expressions. Because the molecular weights of some proteins were close to each other, the primary and secondary antibodies, except for PARP1, were separately probed on different membranes.

2.8. Generation of cardiac-specific Cpt1a knockout mice

Cardiac-specific *Cpt1a* knockout (*Cpt1a*$^{-/-}$) mice were generated and purchased from Biomodel Organism Science & Technology Development (Shanghai, China). In brief, the PGK-Neo-polyA sequence was inserted upstream and the flox sequence was inserted at both ends of exon 3 of *Cpt1a* gene. The resulting chimeric mice were bred to C57BL/6 mice to obtain germline transmission. The neomycin cassette was subsequently excised by breeding with β-actin-Flp mice. Then, *Cpt1a*$^{flp/flp}$ mice were crossed to *Myh6*^{mERcremER} mice (B6.FVB(129)-A1cf.Tg$^{(Myh6\text{-}cre/Esr1*)1Jmk/J}$ (Cat no. 005657), Jackson Laboratory) as we have used before. As described previously[10], Cre recombination and excision of the exon 3 of *Cpt1a* gene in cardiomyocytes were induced by 4-OH-tamoxifen (Sigma) pulse injection. 4-OH-tamoxifen was dissolved in corn oil (Sigma) at a concentration of 5 mg/mL. The mice were intraperitoneally injected 3 times every other day at a dose of 20 mg/kg after MI surgery. Immunostaining for cardiomyocyte proliferation was performed 2 weeks post-MI and echocardiography was performed 4 weeks post-MI. All comparisons used wild-type (WT) littermates as controls, which were also injected with 4-OH-tamoxifen at the same time as the *Cpt1a*$^{-/-}$ mice. To ensure the amount of injury was the same using standard techniques, the infarcted area in WT and *Cpt1a*$^{-/-}$ mice not treated with tamoxifen was also measured after MI for 4 weeks.

2.9. Generation of cardiac-specific Cpt1b knockout mice

Cardiac-specific *Cpt1b* knockout (*Cpt1b*$^{-/-}$) mice were generated and purchased from GemPharmatech (Nanjing, China). In brief, the flox sequence was inserted at both upstream of exon 8 and end of exon 19 of *Cpt1b* gene by using CRISPR/Cas9 technology. Then, *Cpt1b*$^{flp/flp}$ mice were crossed to *Myh6*^{mERcremER} mice (B6.FVB(129)-A1cf.Tg$^{(Myh6\text{-}cre/Esr1*)1Jmk/J}$ (Cat no. 005657), Jackson Laboratory), as we have used before. As described previously[10], Cre recombination and excision of the exons 8−19 of the *Cpt1b* gene in cardiomyocytes were induced by 4-OH-tamoxifen (Sigma) pulse injection. 4-OH-tamoxifen was dissolved in corn oil (Sigma) at a concentration of 5 mg/mL. The mice were intraperitoneally injected 3 times every other day at a dose of 20 mg/kg after MI surgery. Immunostaining for cardiomyocyte proliferation was performed 2 weeks post-MI and echocardiography was performed 4 weeks post-MI. All comparisons used WT littermates as controls, which were also injected 4-OH-tamoxifen at the same time as the *Cpt1b*$^{-/-}$ mice.

2.10. Isolation and culture of cardiomyocytes

Primary cardiomyocytes were isolated from P1, and P7 Sprague−Dawley rats as previously described[2]. Briefly, the hearts were cut into small pieces, and ventricular tissue was digested by 0.8 mg/mL collagenase II (Worthington Biochemical Corporation, Lakewood, NJ, USA) and 1.25 mg/mL trypsin (Sigma) in ADS buffer (0.68% NaCl (*w*/*v*), 0.476% HEPES (*w*/*v*), 0.012% NaH_2PO4 (*w*/*v*), 0.1% glucose (*w*/*v*), 0.04% KCl (*w*/*v*), 0.01% $MgSO_4$ (*w*/*v*), pH 7.35) with shaking at 37 °C. The digestates were pooled and centrifuged at 300×*g* for 5 min and resuspended in plating medium with 10% fetal bovine serum (Gibco BRL, Grand Island, NY, USA). The cells were then plated on 100 mm tissue culture dishes (Jet, Guangzhou, China), and incubated for 60 min at 37 °C in 5% CO_2 to separate adherent cardiac fibroblasts. Then, P1 or P7 primary cardiomyocytes were plated on laminin-coated chamber slides (Nunc, Thermo Fisher Scientific) and incubated for 2 days at 37 °C in 5% CO_2 to allow cellular attachment. Two days later, the cardiomyocytes were washed with PBS, and the plating medium was replaced with maintenance medium (79.5% Dulbecco's modified Eagle's medium (DMEM), 19.5% medium 199, 1% fetal bovine serum (FBS)), supplemented with 1% penicillin/streptomycin (Solarbio). Then, *Cpt1a, Cpt1b, Gck*, *Dusp1*, *Dusp4*, *Dusp12* or *Map2k3* siRNA transduction was performed. After siRNA transduction for 24 h, the medium was replaced with maintenance medium supplemented with 1% penicillin/streptomycin.

2.11. Drug and siRNA administration

To explore the role of fatty acid metabolism in the proliferation of cultured cardiomyocyte, ETX (40 μmol/L, MedChemExpress) was used to inhibit fatty acid metabolism.

The role of *Cpt1a*, *Cpt1b*, *Gck*, *Dusp1*, *Dusp4*, *Dusp12*, and *Map2k3* in cardiomyocyte proliferation was studied using rat-specific siRNA of *Cpt1a*, *Cpt1b*, *Gck*, *Dusp1*, *Dusp4*, *Dusp12*

and *Map2k3* to decrease their gene expressions. Scramble RNA was used as negative control. The final siRNA concentration was 50 nmol/L in all experiments. All siRNAs were synthesized at RiboBio Co., Ltd. (Guangzhou, China).

2.12. Seahorse glycolysis measurement

Neonatal cardiomyocytes media were replaced with bicarbonate and glucose-free DMEM, containing 2 mmol/L glutamine. The extracellular acidification rate (ECAR) was measured using an XFe24 Extracellular Flux Analyzer (Agilent Technologies, Santa Clara, CA, USA). Triplicate pre-injection readings were taken to establish a baseline, followed by triplicate readings after sequential treatment with 20 mmol/L glucose, 2 μmol/L oligomycin, and 100 mmol/L 2-deoxy-D-glucose. Normalization to 10 μg protein/well was performed by extracting protein lysates from each well and measuring protein concentration, using a bicinchoninic acid (BCA) protein assay kit (Solarbio, Beijing, China), following the manufacturer's protocol. The glycolysis parameters were calculated as Eqs. (2) and (3):

$$\text{Glycolysis} = (\text{Maximal ECAR before oligomycin injection}) - (\text{Non-glycolytic acidification}) \quad (2)$$

$$\text{Glycolytic capacity} = (\text{Maximal ECAR}) - (\text{Non-glycolytic acidification}) \quad (3)$$

2.13. Seahorse fatty acid oxidation measurement

The cardiomyocytes were starved for 24 h in substrate-limited medium (DMEM, 0.5 mmol/L glucose, 1.0 mmol/L glutamine, 0.5 mmol/L L-carnitine, 1% FBS) and replaced with FAO assay medium (Seahorse XF DMEM with 2.5 mmol/L glucose and 0.5 mmol/L L-carnitine). After incubation at 37 °C in a CO_2-free chamber for 1 h, the cardiomyocytes were treated with BSA or palmitic acid. The oxygen consumption rate (OCR) was measured using the XFe24 Extracellular Flux Analyzer. Quadruplicate or sextuplicate pre-injection readings were recorded to establish a baseline and cardiomyocytes were sequentially treated with 2 μmol/L oligomycin, 2 μmol/L carbonyl cyanide-4-(trifluoromethoxy) phenylhydrazone (FCCP), and a mixture of 1 μmol/L antimycin A and 1 μmol/L rotenone. Normalization to 10 μg protein/well was performed by extracting protein lysates from each well and measuring the protein concentration, using BCA protein assay kit (Solarbio), following the manufacturer's protocol. The respiration parameters were calculated as Eqs. (4) and (5):

$$\text{Maximal respiration} = (\text{Maximal OCR}) - (\text{Non-mitochondrial respiration}) \quad (4)$$

$$\text{Spare respiration capacity} = (\text{Maximal OCR}) - (\text{Maximal OCR before oligomycin injection}) \quad (5)$$

2.14. Measurement of oxygen consumption rate in isolated adult cardiomyocytes

Cardiomyocytes were isolated from WT and *Cpt1a*$^{-/-}$ mice *via* Langendorff perfusion, as described previously[10]. The cardiomyocytes were seeded onto laminin pre-coated XFe24 well plates (20,000/well) and initially placed in DMEM, supplemented with penicillin-streptomycin (100 units/mL) and 5% FBS at 37 °C in 5% CO_2-humidified atmosphere for 1 h. The medium was changed to XF Assay Medium supplemented with 25 mmol/L glucose, 2 mmol/L glutamine, and 1 mmol/L sodium pyruvate, incubated at 37 °C in a CO_2-free chamber for 1 h. The OCR was measured using the XFe24 Extracellular Flux Analyzer. Triplicate pre-injection readings were recorded to establish baseline and cardiomyocytes were sequentially treated with 2 μmol/L oligomycin, 2 μmol/L FCCP, and a mixture of 1 μmol/L antimycin A and 1 μmol/L rotenone.

2.15. Isolation of cardiomyocytes from fixed hearts

The isolation of cardiomyocytes from fixed hearts was performed as previously described[14]. Briefly, P14 and post-myocardial hearts, treated with vehicle (saline) and ETX, were harvested and fixed in 4% PFA at 4 °C for 3 h. Then, the samples were digested by collagenase D (2.4 mg/mL, Roche) and B (1.8 mg/mL, Roche) in PBS buffer for 12 h at 37 °C. The supernatant was centrifuged to obtain the isolated cardiomyocytes. The remaining heart tissues were minced in blocks of 1 mm^3 and this process was repeated until no more cardiomyocytes were recovered. The number of cardiomyocytes was counted using a hemocytometer.

2.16. Time-lapse imaging microscopy for observing cytokinesis of adult cardiomyocytes

Mouse adult cardiomyocytes were isolated and cultured as previously described[10]. In brief, the hearts of GFP transgenic mice (C57BL/6-Tg$^{CAG-GFP}$), purchased from the Shanghai Model Organisms Center, were digested *via* Langendorff perfusion of a Tyrode solution containing collagenase II (290 U/mL), pH 7.4. After 10 min of digestion, the ventricles were minced, and isolated cardiomyocytes were equilibrated in Tyrode solutions, serially supplemented with 125−250 μmol/L $CaCl_2$ (10 min for each step). For mixed co-culture study, GFP positive adult cardiomyocytes were seeded on top of a feeding layer of P1 cardiomyocytes. The adult cardiomyocytes and the feeder cell types were plated at a ratio of 1:20. Then, immediately, the co-culture plate was placed in the humidified cell culture chamber of Olympus IX83 inverted microscope in 5% CO_2 at 37 °C. 100 fields of 10 × objective lens were randomly selected, and the positions were marked with the "position-list" tool in the microscopy software. The time-lapse images were taken at intervals of 1 h for 7 days. Time-lapse movies were generated at the end of each experiment and exported as. AVI files.

2.17. Mosaic analysis with double markers (MADM) mice

As shown in Supporting Information Fig. S1, for lineage tracing and analyzing cytokinesis of adult cardiomyocytes, we used MADM mice which required the crossing of transgenic lines to generate the ubiquitous labeling obtained from JAX labs: Igs2tm2$^{(ACTBtdTomato,-EGFP)Zng/J}$ (Cat no. 022977); Igs2tm1$^{(ACTB-EGFP,-tdTomato)Zng/J}$ (Cat no. 022976). To determine the generation of new cardiomyocytes, the MADM mice were crossed to B6.FVB(129)-A1cf.Tg$^{(Myh6-cre/Esr1*)1Jmk/J}$ (Cat no. 005657) to generate *Myh6*^{mERcremER}-MADM, as previously described[2,14,15]. The mice were intraperitoneally injected with 4-OH-tamoxifen, 20 mg/kg every day for 2 weeks, after sham or MI surgery.

2.18. Plasmid transfection

p38 MAPK WT, p38 MAPK T180A/Y182A, PARP1 WT, and PARP1 E988K plasmid were generated by and purchased from Genechem (Shanghai, China). Plasmid transduction was performed with lipofectamine® LTX & PLUS™ reagent, according to the manufacturer's protocol. Briefly, P7 primary cardiomyocytes were plated on laminin-coated 6-well plates or chamber slides. The seeded cardiomyocytes were transfected when they were 70%−90% confluent. Diluted lipofectamine LTX reagents in Opti-MEM medium (Gibco) were mixed and the master mix of plasmid was prepared by diluting plasmid DNA in Opti-MEM medium. Then, the PLUS™ reagent (2 μL/μg DNA) was added and mixed well. The diluted plasmid DNA was added to diluted lipofectamine LTX reagent (1:1 ratio) and incubated for 5 min at room temperature. The plasmid DNA−lipid complex was added to the cells at the final plasmid DNA concentration of 2.5 μg/mL. After the cells were incubated for 24 h at 37 °C, the media containing complex was replaced by DMEM containing 10% FBS. After the additional incubation for 24 h transfected cardiomyocytes were analyzed.

2.19. Immunoprecipitation

Equal amounts of cell lysates (200 μg protein per sample) were incubated with the primary antibodies or IgG (2 μg) as negative control (Beyotime, Shanghai, China) overnight at 4 °C. The primary antibodies included anti-DUSP1 (2 μg) and anti-PARP1 (2 μg). The immunocomplexes were isolated with protein A+G agarose (Beyotime) for 2 h at room temperature and then washed three times with PBS. After boiling in loading buffer, the immunoprecipitates were subjected to immunoblotting with the appropriate antibodies, including anti-DUSP1 (1:1000), anti-Poly/Mono-ADP ribose (1:1000), and anti-p38 MAPK (1:1000).

2.20. Untargeted metabolomics

Fifty mg of P14 heart tissue after treatment with or without ETX were placed into an EP tube. After the extraction procedure, the metabolites and quality control reagent were prepared for LC−MS/MS analyses, using an UHPLC system (1290, Agilent Technologies) with a UPLC HSS T3 column (2.1 mm × 100 mm, 1.8 μm) coupled to Q Exactive (Orbitrap MS, Thermo Fisher Scientific). After LC−MS/MS analyses, the raw data were converted to the mzXML format using ProteoWizard and processed by MAPS software (version 1.0). The preprocessing results generated a data matrix that consisted of the retention time (RT), mass-to-charge ratio (*m*/*z*) values, and peak intensity. In-house MS2 database was used for the identification of metabolites.

2.21. Generation and administration of adeno-associated virus (serotype 9)

cDNA constructs targeting mouse *Parp1* genes and adeno-associated virus serotype 9 (AAV9) were generated and purchased from OBio Technology Co., Ltd. (Shanghai, China). cDNA constructs targeting mouse *p38 Mapk*, *p38 Mapk* (T180A/Y182A) genes, and AAV9 were generated and purchased from Hanbio Biotechnology Co., Ltd. (Shanghai, China). Briefly, mouse *Parp1*, *p38 Mapk*, and *p38 Mapk* (T180A/Y182A) cDNA were, respectively, cloned into ITR-containing AAV plasmid along with 3 × Flag under cTNT promoter. AAV9 was packaged using a plasmid encoding Rep-Cap sequence. AAV9 was packaged in AAV-293 cells with AAV9 Rep-Cap along with an AAV Helper-Free System (Agilent Technologies, Santa Clara, CA, USA) and then purified and concentrated by CsCl density gradient centrifugation. AAV9 titer was determined by quantitative PCR. In AAV9 administration, 1×10^{10} viral genomes (vg) diluted with sterile 0.9% NaCl in 10 μL volume were used. After the ligation of the LAD, 10 μL AAV9 was immediately injected into myocardium around the ligation point for 4 times. AAV9 without cDNA was also injected as negative control in the experiments. After 4 weeks, the AAV9 infection rate and cardiomyocyte proliferation rate were investigated.

2.22. EdU analysis

Adult mice were injected with 50 mg/kg EdU (reconstituted in saline) intraperitoneally once daily for 1 week after MI surgery, and the hearts were harvested 4 weeks after MI. Cardiomyocytes were isolated from freshly harvested hearts which were fixed in 4% PFA at 4 °C for 24 h. Then, the samples were digested by collagenase D (2.4 mg/mL, Roche) and B (1.8 mg/mL, Roche) in PBS buffer for 12 h at 37 °C. The supernatant was centrifuged to obtain the isolated cardiomyocytes. The remaining heart tissues were minced in blocks of 1 mm^3 and this process was repeated until no more cardiomyocytes were obtained. EdU labeling of the cardiomyocytes was assessed by using the Click-iT EdU Alexa Fluor 555 Imaging Kit (Thermo Fisher Scientific). Then, DAPI was used to stain nuclei. Nucleation of EdU-positive (EdU^+) cardiomyocytes was manually counted, and the ploidy of EdU^+ cardiomyocyte nuclei was determined by normalizing the DAPI intensity of cardiomyocyte nuclei to that of non-cardiomyocyte nuclei in the same field, as previously described[16].

2.23. Statistics

The data are expressed as mean ± standard error of mean (SEM). All data collected and analyzed were assumed to be distributed normally. The experiments were not randomized, and the investigators were not blinded to allocation during experiments and outcome assessment except for all echocardiographic studies. Two groups were compared using the Student's unpaired *t*-test. For multiple-group comparisons, one-way ANOVA was performed followed by the Holm−Sidak test. A value of $P < 0.05$ was considered statistically significant.

3. Results

3.1. Cardiac fuel metabolic reprogramming determined the proliferation of neonatal cardiomyocytes

The mammalian cardiomyocyte's proliferative capacity is known to decrease sharply during the first postnatal week, along with metabolic reprogramming from glycolysis to FAO. An mRNA array was performed in mouse hearts between normal P1 and P7, which showed numerous differentially expressed genes. According to Gene Ontology (GO) analyses, those genes related to cell metabolism and cell cycle/cell division ranked in the top changes in gene expressions (Fig. 1A and B). Among the metabolic enzymes related to glycolysis, GCK expression was significantly decreased, while among the metabolic enzymes related to FAO, CPT1

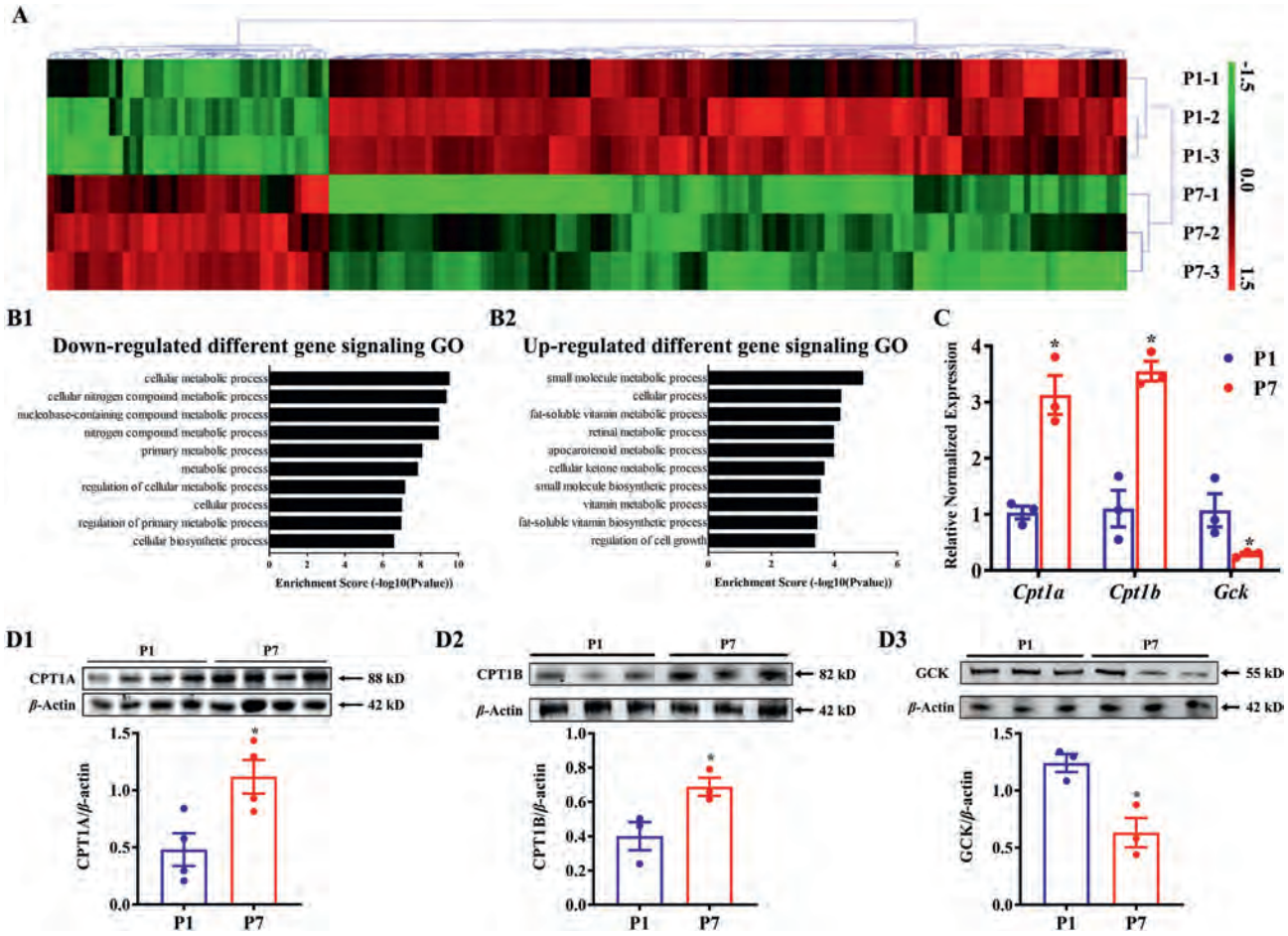

Figure 1 Microarray analysis reveals that metabolism-related genes expression are changed after birth in mice hearts. (A) Heat map of differentially expressed genes in P7 heart as compared with P1. (B) The results of GO analysis of differentially expressed genes are shown. (C) *Cpt1a*, *Cpt1b,* and *Gck* gene expression in P1 and P7 hearts ($n = 3$, $^*P < 0.05$ *vs.* P1). (D) CPT1A, CPT1B, and GCK protein expression in P1 and P7 hearts ($n = 4$ for CTP1A; $n = 3$ for CPT1B and GCK; $^*P < 0.05$ *vs.* P1). Error bars indicate SEM.

expression was significantly increased (Fig. 1C and D, Supporting Information Fig. S2A).

We next tested how glycolysis or FAO influences proliferation in cultured neonatal cardiomyocytes. GCK was silenced with siRNA in P1 cardiomyocytes (Fig. S2B). The successful inhibition of glycolysis by *Gck*-siRNA (si*Gck*) was confirmed by Seahorse analysis in P1 cardiomyocytes. The result showed that si*Gck*-treated cardiomyocytes exhibited lower levels of glycolysis and glycolytic capacity which indicated the successful inhibition of glucose utilization (Fig. 2A). Meanwhile, we found that si*Gck* inhibited the proliferation of P1 cardiomyocytes, indicated by decreased $Ki67^+$ and $PH3^+$ staining (Fig. 2B and C).

In addition to GCK, we also used CPT1 siRNA to knock down CPT1 expression. Seahorse analysis showed that *Cpt1a*-siRNA (si*Cpt1a*) or *Cpt1b*-siRNA (si*Cpt1b*) decreased the maximal respiration and spare respiratory capacity in the group that included palmitic acid which proved the inhibition of fatty acid utilization in P7 cardiomyocytes (Fig. 2D and E, Fig. S2B). si*Cpt1a* and si*Cpt1b* also promoted P7 cardiomyocyte proliferation, indicated by the increase in $Ki67^+$ and $PH3^+$ staining (Fig. 2F and G). Our data show that the inhibition of glycolysis blocked cardiomyocyte proliferation, while inhibition of FAO stimulated cardiomyocyte proliferation. Therefore, CPT1 may be a treatment target for manipulating metabolic reprogramming and promoting cardiac regeneration.

3.2. Cardiac-specific Cpt1 knockout promoted cardiomyocyte proliferation and improved cardiac function post-MI

CPT1 controls the mitochondrial uptake of long-chain acyl-CoAs. To determine if cardiac metabolic reprogramming stimulates the proliferation in adult cardiomyocytes and exerts a therapeutic effect against MI, we generated 4-OH-tamoxifen-inducible, cardiac-specific *Cpt1a* knockout mice $Myh6^{mERcremER}$-$Cpt1a^{flp/flp}$ (Fig. 3A and Supporting Information Fig. S3A−S3C). The cardiomyocytes in these mice had a decrease in maximal respiration and spare respiratory capacity (Fig. S3D). The $Cpt1a^{-/-}$ and WT mice were subjected to MI, induced by the ligation of the LAD coronary artery (Fig. S3E). Immunostaining for cardiomyocyte proliferation was performed 2 weeks post-MI and echocardiography was performed 4 weeks post-MI. MI decreased cardiac function, indicated by decreased left ventricular ejection fraction (LVEF) and left ventricular fraction shortening (LVFS), and increased left ventricular internal dimension at end-diastole (LVIDd) and end-systole (LVIDs) and left ventricular end-diastolic (LVEDV) and end-systolic volumes (LVESV) at 4

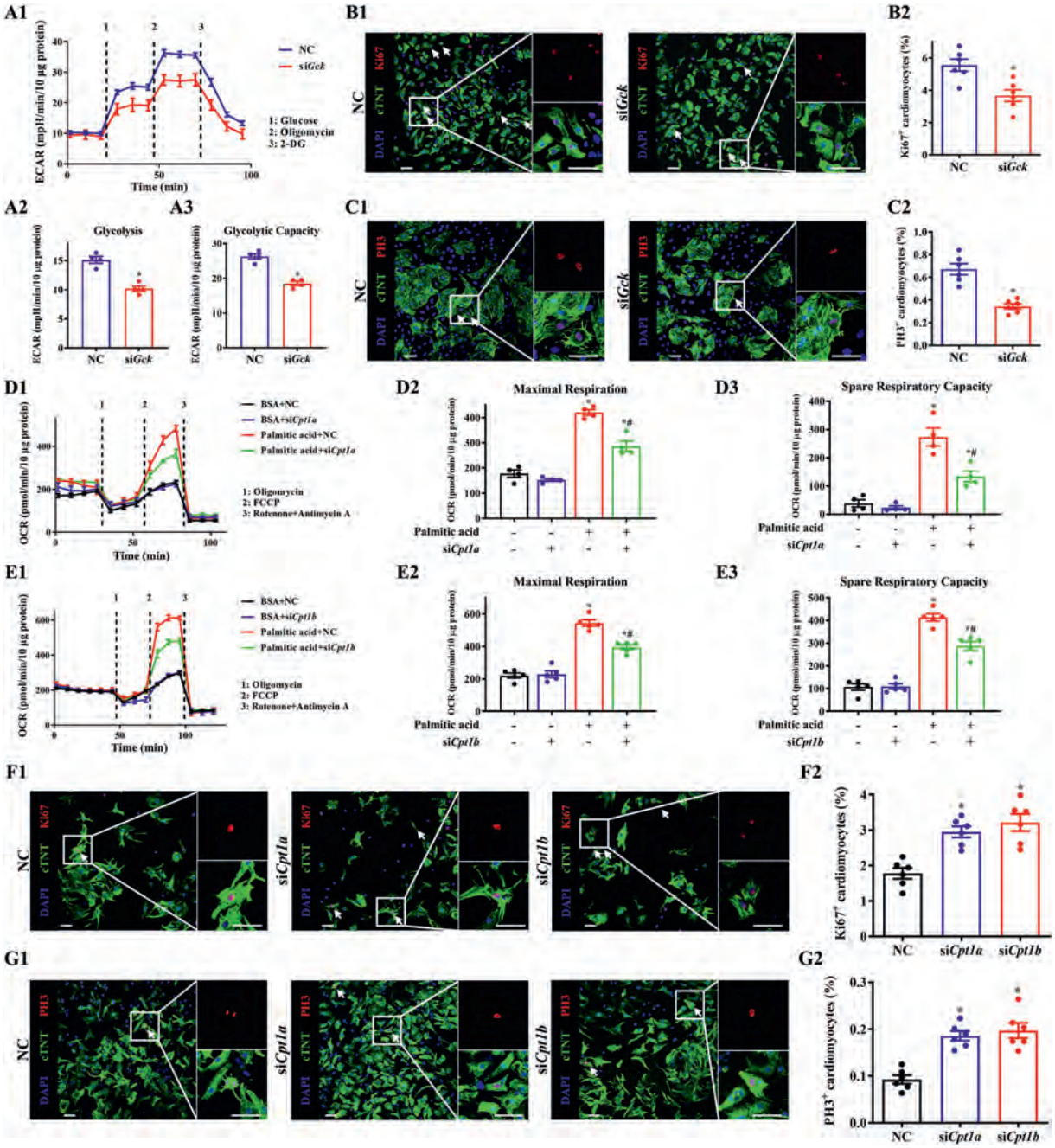

Figure 2 Modulating cardiac metabolic reprogramming reverses the proliferation of neonatal cardiomyocytes. (A) Measurement of extracellular acidification rate (ECAR) in neonatal cardiomyocytes. Dotted lines indicate the time points of adding glucose, oligomycin, and 2-deoxy glucose (2-DG). Glycolysis and glycolytic capacity in neonatal cardiomyocytes are decreased after si*Gck* treatment compared with negative control (NC) ($n = 4$, $^{*}P < 0.05$ *vs.* NC). (B, C) Co-immunostaining of anti-Ki67, anti-PH3, and anti-cardiac troponin T (cTNT) antibodies shows that *Gck* siRNA (si*Gck*) decreases the ratio of $Ki67^{+}$ (red, white arrow) and $PH3^{+}$ (red, white arrow) in P1 cardiomyocytes, relative to NC ($n = 6$, $^{*}P < 0.05$ *vs.* NC). (D, E) Measurement of OCR in P7 cardiomyocytes following 24 h of glucose starvation. Cardiomyocytes were sequentially incubated with BSA or palmitic acid. Dotted lines indicate the time points of adding oligomycin, FCCP, and rotenone + antimycin A. Maximal respiration and spare respiratory capacity in P7 cardiomyocytes are decreased after *Cpt1a* siRNA (si*Cpt1a*) or *Cpt1b* siRNA (si*Cpt1b*) treatment ($n = 4$ for si*Cpt1a* group and $n = 5$ for si*Cpt1b* group, $^{*}P < 0.05$ *vs.* BSA+NC; $^{\#}P < 0.05$ *vs.* Palmitic acid + NC). (F, G) Co-immunostaining, using anti-cTNT (green) and anti-Ki67 or anti-PH3 (red) antibodies, shows that either si*Cpt1a* or si*Cpt1b* increases the ratio of $Ki67^{+}$ (red, white arrow) or $PH3^{+}$ (red, white arrow) in P7 cardiomyocytes ($n = 6$, $^{*}P < 0.05$ *vs.* NC). Scale bars = 50 μm. Error bars indicate SEM.

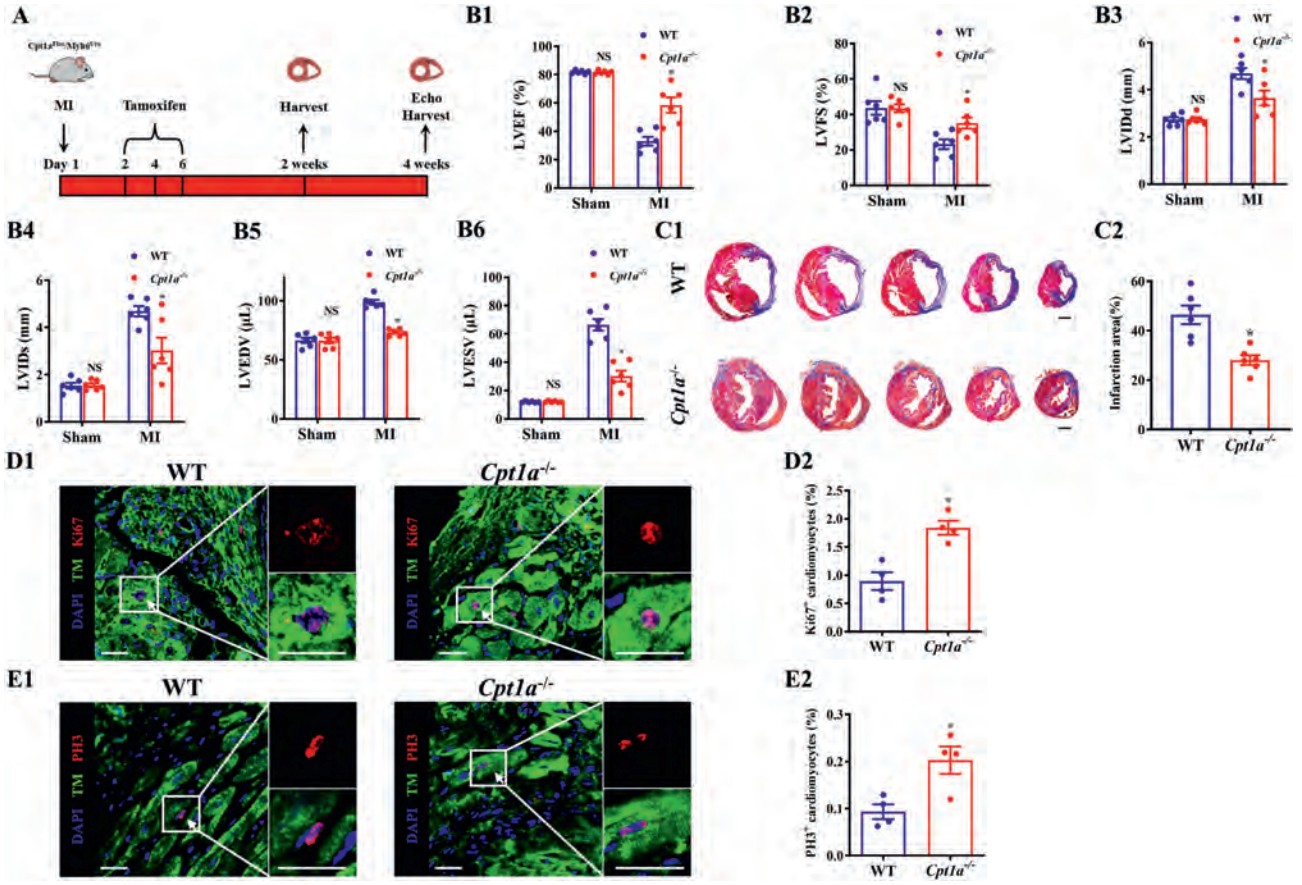

Figure 3 Cardiac-specific *Cpt1* knockout promotes cardiomyocyte proliferation and cardiac function post-MI. (A) MI was induced in adult $Cpt1a^{-/-}$ mice. After 4-OH-tamoxifen injection every other day for 1-week, cardiac proliferation was evaluated at 2 weeks, while cardiac function was assessed by echocardiography at 4 weeks after MI. (B) LVEF, LVFS, LVIDd, LVIDs, LVEDV and LVESV at 4 weeks after Sham or MI were measured in $Cpt1a^{-/-}$ and WT mice ($n = 6$, $^*P < 0.05$ *vs.* WT). (C) The infarcted area of the heart in $Cpt1a^{-/-}$ and WT mice, 4 weeks after MI ($n = 6$, $^*P < 0.05$ *vs.* WT; Scale bars = 1 mm). (D, E) Co-immunostaining, using anti-tropomyosin (TM) (green) and anti-Ki67 or anti-PH3 (red) antibodies in $Cpt1a^{-/-}$ and WT mice, shows that the ratio of $Ki67^+$ (red, white arrow) or $PH3^+$ (red, white arrow) in cardiomyocytes is increased in $Cpt1a^{-/-}$ mice after MI for 2 weeks. The $PH3^+$ non-cardiomyocyte was showed in WT group of Fig. 2E ($n = 4$, $^*P < 0.05$ *vs.* WT). Scale bars = 20 μm. Error bars indicate SEM.

weeks post-MI, determined by echocardiography, which was partially rescued by *Cpt1a* knockout (Fig. 3B). Moreover, the MI-induced infarct size, determined by Masson's trichrome staining, was decreased in $Cpt1a^{-/-}$ mice, relative to WT littermates (Fig. 3C). Furthermore, $Ki67^+$ and $PH3^+$ expressions in cardiomyocytes in the infarct border zone post-MI were increased in $Cpt1a^{-/-}$ mice relative to WT controls (Fig. 3D and E). Besides, apoptosis [terminal-deoxynucleoitidyl transferase mediated nick end labeling positive ($TUNEL^+$) rate] and fibrosis (Masson staining) were also decreased in $Cpt1a^{-/-}$ mice (Fig. S3F and S3G). These results indicate that cardiac-specific deletion of *Cpt1a* increased cardiomyocyte proliferation and improved cardiac function in adult mice with MI.

To provide additional confirmatory data, we also generated 4-OH-tamoxifen-inducible, cardiac-specific *Cpt1b* knockout mice $Myh6^{mERcremER}$-$Cpt1b^{flp/flp}$ (Supporting Information Fig. S4A and S4B). Consistent with the results from $Cpt1a^{-/-}$ mice, cardiac-specific deletion of *Cpt1b* also increased cardiomyocyte proliferation and improved cardiac function in adult mice after MI (Fig. S4C−S4F).

3.3. The CPT1 inhibitor etomoxir increased cardiomyocyte proliferation in normal postnatal mice and exerted a therapeutic effect on MI in adult mice

Etomoxir (ETX) is an irreversible inhibitor of mitochondrial CPT1 on the inner face of the outer mitochondrial membrane, which has been demonstrated to switch energy metabolism from fatty acids to glucose oxidation in the mouse heart[17]. However, it is not known if ETX can stimulate cardiomyocyte proliferation. Consistent with the siRNA result, *in vitro* experiments showed that ETX (40 μmol/L) increased the proliferation in P7 mouse cardiomyocytes, determined by $Ki67^+$ and $PH3^+$ staining (Supporting Information Fig. S5A and S5B). As we have reported[10], an *in vitro* system with time-lapse microscopy can quantify adult cardiomyocyte cytokinesis. We used time-lapse microscopy to verify the cytokinesis rate of adult cardiomyocytes. The data show that the cytokinesis rates of adult cardiomyocytes were significantly increased by ETX treatment (Fig. S5C). In normal postnatal mice, ETX was intraperitoneally injected (20 mg/kg/day) for 1 week starting on Day 7 (P7) after

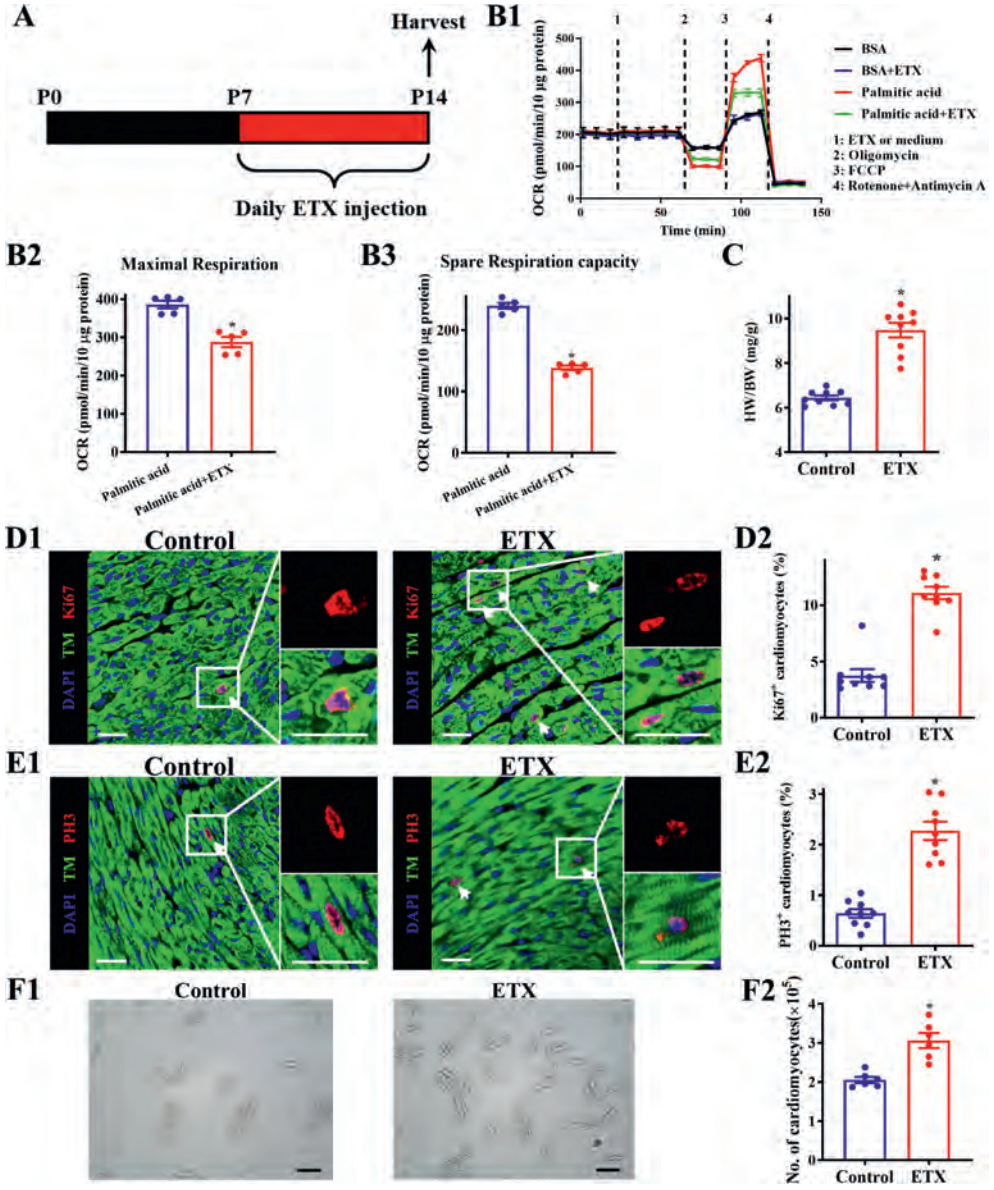

Figure 4 CPT1 inhibitor etomoxir increases cardiomyocyte proliferation in normal postnatal mice. (A) ETX (20 mg/kg) was injected subcutaneously, daily for one week in P7 mice; the hearts were harvested at P14. (B) Measurement of OCR in P7 cardiomyocytes following 24 h of glucose starvation. Cardiomyocytes were sequentially incubated with BSA or palmitic acid. Dotted lines indicate the time points of adding BSA, BSA+ETX, oligomycin, FCCP, and rotenone + antimycin A. Maximal respiration and spare respiratory capacity in P7 cardiomyocytes are decreased after ETX treatment ($n = 5$, $^*P < 0.05$ *vs.* Palmitic acid). (C) The ratio of heart weight and body weight (HW/BW) in mice with or without ETX treatment ($n = 9$, $^*P < 0.05$ *vs.* Control). (D, E) Co-immunostaining, using anti-tropomyosin (TM) (green) and anti-Ki67 or anti-PH3 (red) antibodies in ETX-treated and vehicle-treated (Control) hearts, shows that ETX treatment increases the ratio of $Ki67^+$ (red, white arrow) or $PH3^+$ (red, white arrow) in P14 hearts ($n = 9$, $^*P < 0.05$ *vs.* Control). (F) Representative images of isolated cardiomyocytes and quantification of the number of cardiomyocytes from P14 mice after ETX or vehicle (Control) treatment for one week. Approximately 1000 cardiomyocytes per group were counted using a hemocytometer ($n = 6$, $^*P < 0.05$ *vs.* Control). Scale bars = 20 μm. Error bars indicate SEM.

birth, and the hearts were harvested at P14 (Fig. 4A). The successful inhibition of FAO by ETX was proved by Seahorse analysis (Fig. 4B). ETX injection increased the heart weight to body weight ratio (HW/BW) without causing any change in cardiomyocyte size (Fig. 4C and Fig. S5D). The percentages of $Ki67^+$ and $PH3^+$ cardiomyocytes were significantly increased by ETX treatment (Fig. 4D and E). We also counted the number of cardiomyocytes by isolation of cardiomyocytes from the P14 heart after ETX treatment for one week. The results showed that the number of cardiomyocytes was significantly increased, almost 50%, by ETX treatment (Fig. 4F). The numbers of cardiomyocytes in culture plate were also counted. The result showed that the total number of cardiomyocytes in the culture plate was significantly increased after ETX treatment (Fig. S5E). These results indicate that ETX can induce the proliferation of post-natal cardiomyocytes.

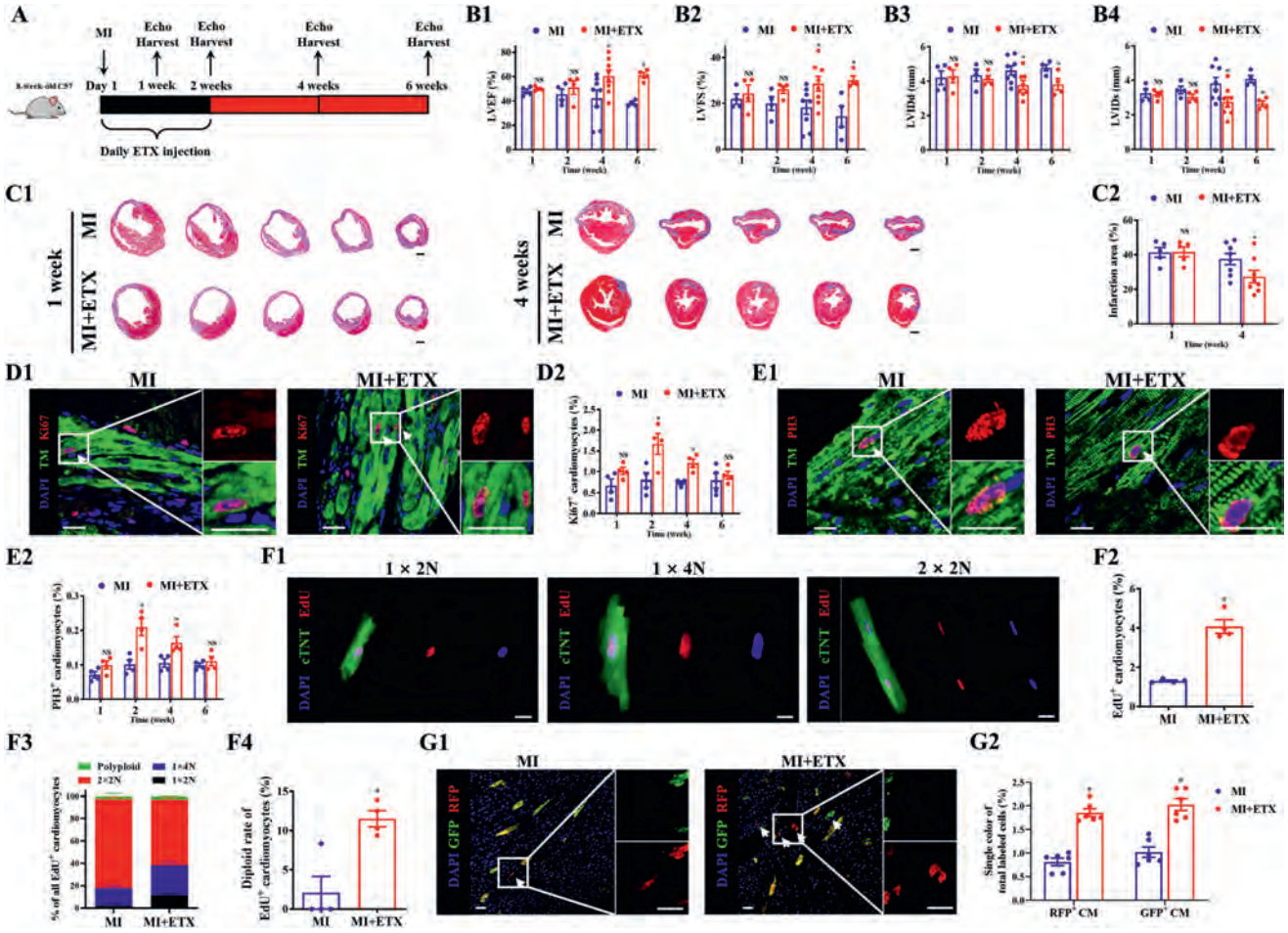

Figure 5 CPT1 inhibitor etomoxir increases cardiomyocyte proliferation and exerts a therapeutic effect against MI in adult mice. (A, B) Adult mice were treated with ETX immediately after MI. Cardiac proliferation was measured after treatment for 1, 2, 4 and 6 week(s), while cardiac function was measured by echocardiography after treatment for 1, 2, 4 and 6 week(s) ($n = 4$ for 1, 2 and 6 week(s), $n = 8$ for 4 weeks, $^*P < 0.05$ *vs.* MI). (C) The infarcted area of the heart with or without ETX treatment for 1 week and 4 weeks after MI is shown ($n = 4$ for 1 week and $n = 8$ for 4 weeks, $^*P < 0.05$ *vs.* MI, NS = Not significant; Scale bars = 1 mm). (D, E) Co-immunostaining, using anti-cTNT (green) and anti-Ki67 or anti-PH3 (red) antibodies in MI and MI+ETX mice, shows that the ratio of $Ki67^+$ (red, white arrow) or $PH3^+$ (red, white arrow) in ETX-treated (MI+ETX) and vehicle-treated (MI) adult hearts after MI for 1, 2, 4 and 6 week(s), shows that ETX treatment increases the ratio of $Ki67^+$ (red, white arrow) or $PH3^+$ (red, white arrow) in adult hearts after MI for 2 and 4 weeks ($n = 4$, $^*P < 0.05$ *vs.* MI, NS = Not significant). (F) Representative images of EdU^+ diploid ($1 \times 2n$) and tetraploid (both $2 \times 2n$ and $1 \times 4n$) cardiomyocytes. Quantification of the percentage of EdU^+ rate, diploid rate and tetraploid rate of cardiomyocytes were presented ($n = 4$, $^*P < 0.05$ *vs.* MI). (G) Representative immunofluorescence and quantification of single-labeled (red or green, white arrow) cardiomyocytes in MADM mice after MI for 4 weeks ($n = 6$, $^*P < 0.05$ *vs.* Control). Scale bars = 20 μm. Error bars indicate SEM.

In adult mice, ETX was immediately injected after MI for 2 weeks (Fig. 5A). MI decreased LVEF and LVFS and increased LVIDd, LVIDs, LVEDV and LVESV 4 weeks post-MI, which were mitigated by ETX (Fig. 5B, Supporting Information Fig. S6A and S6B). In addition, ETX treatment reduced the MI-induced infarct size (Fig. 5C). In the infarct border zone, ETX significantly increased the number of $Ki67^+$ and $PH3^+$ cardiomyocytes (Fig. 5D and E, Fig. S6C and S6D), decreased the apoptosis of cardiomyocytes without affecting cardiomyocyte size (Fig. S6E and S6F). In an additional study, to label the cardiomyocytes, EdU was injected during the first week after MI and revealed a 3.1-fold increase in EdU^+ cardiomyocytes 4 weeks after MI with ETX treatment (Fig. 5F1 and 5F2). Because EdU^+ and diploid cardiomyocytes indicate the completion of cytokinesis, we further counted the ploidy of EdU^+ cardiomyocytes. There was a 5.5-fold increase in diploid in EdU^+ cardiomyocytes suggesting that the complete division of cardiomyocytes was increased after ETX treatment (Fig. 5F3 and 5F4). Additionally, we used a lineage-tracing system in which we crossed cardiomyocyte-specific *Myh6*^{mERcremER} mice with MADM mice to examine cardiomyocyte division. Assessment of single-colored green or red cardiomyocytes confirmed that ETX treatment after MI resulted in more cardiomyocyte formation in both the infarct border zone and remote zone (Fig. 5G and Fig. S6G–S6J). These results indicate that ETX induced cardiomyocyte proliferation, reduced cardiomyocyte apoptosis, and improved cardiac function post-MI in adult mice.

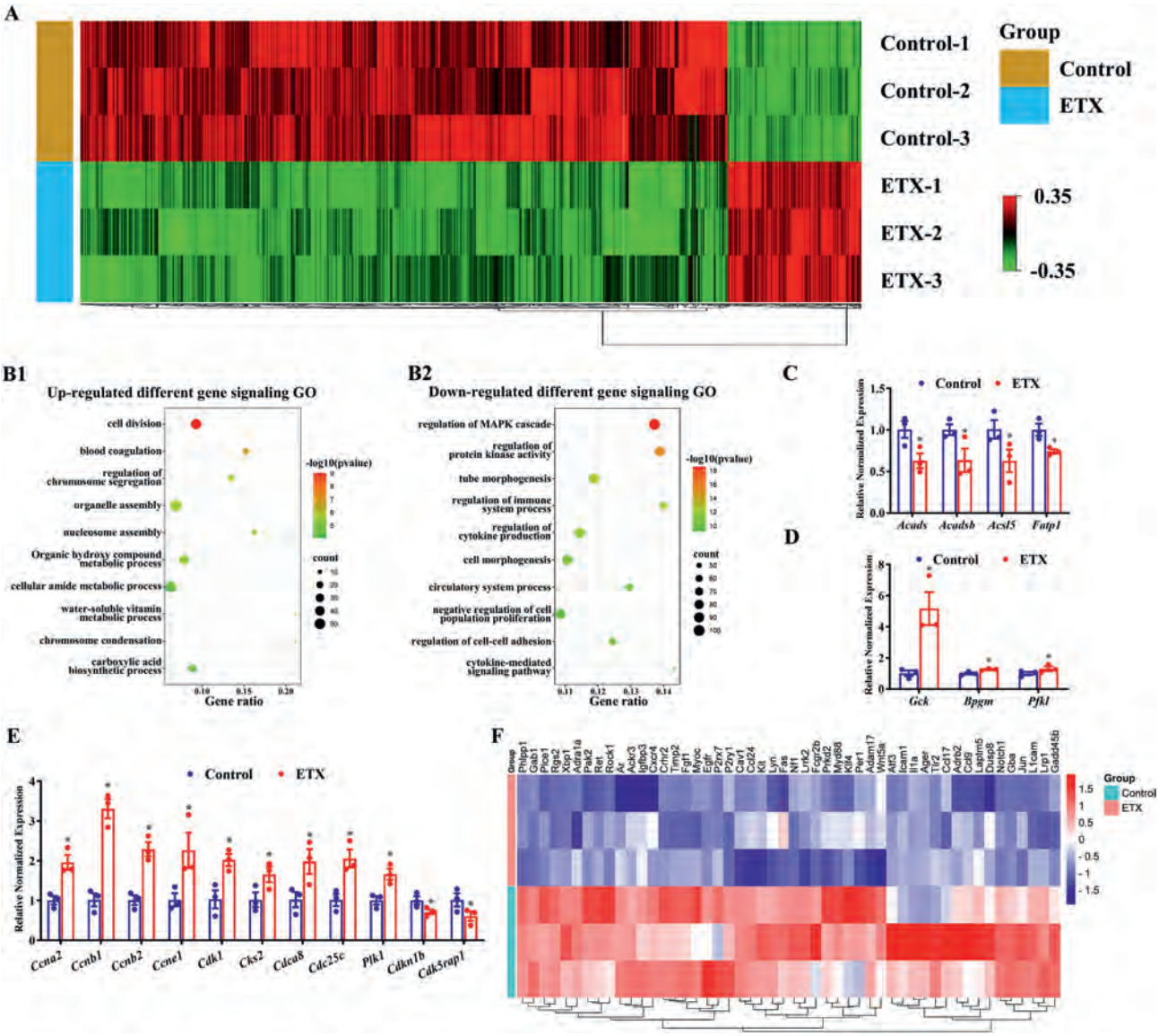

Figure 6 Microarray analysis reveals that p38 MAPK signaling pathway is involved in CPT1 inhibition induces cardiomyocytes proliferation. (A) Heat map of differentially expressed genes in hearts from ETX-treated or control mice. (B) The results of GO analysis of up- or down-regulated genes. (C) ETX down-regulated fatty acid metabolism regulating genes, including acyl-Coenzyme A dehydrogenase, short chain (*Acads*), acyl-Coenzyme A dehydrogenase, short/branched chain (*Acadsb*), acyl-CoA synthetase long chain family member 5 (*Acsl5*) and fatty acid transporter, member 1 (*Fat1p1*) ($n = 3$, $^*P < 0.05$ *vs.* Control). (D) ETX up-regulated glycolysis regulating genes, including *Gck*, 2,3-bisphosphoglycerate mutase (*Bpgm*), and phosphofructokinase-1 (*Pfk1*) ($n = 3$, $^*P < 0.05$ *vs.* Control). (E) Cyclin A2 (*Ccna2*), cyclin B1 (*Ccnb1*), cyclin B2 (*Ccnb2*), cyclin E1 (*Ccne1*), cyclin-dependent kinase 1 (*Cdk1*), CDC28 protein kinase regulatory subunit 2 (*Cks2*), cell division cycle associated 8 (*Cdca8*), cell division cycle 25C (*Cdc25c*), polo-like kinase 1 (*Plk1*), cyclin-dependent kinase inhibitor 1B (*Cdkn1b*), and CDK5 regulatory subunit associated protein 1 (*Cdk5rap1*) gene expression with ETX or without (Control) ETX treatment ($n = 3$, $^*P < 0.05$ *vs.* control). (F) Heat map of differentially expressed genes related to p38 MAPK signaling after ETX treatment. Error bars indicate SEM.

3.4. CPT1 inhibition induced cardiomyocytes proliferation via p38 MAPK signaling pathway

To explore further the mechanism of ETX-induced cardiomyocyte proliferation, mRNA microarray analysis was performed in mouse hearts. ETX was injected daily for 1 week after P7 and the hearts were harvested at P14 for mRNA microarray analysis. The assay identified 2325 up-regulated and 2320 down-regulated genes, with at least a 1.2-fold change in ETX-treated hearts. GO analysis suggested that 130 genes are involved in metabolic pathways (Fig. 6A and B). The decrease in fatty acid metabolism-regulating genes and increase in glycolysis-regulating genes were confirmed by qPCR (Fig. 6C and D). Ninety genes are cell cycle-related genes, and qPCR confirmed the increase of pro-proliferative genes, *e.g.*, *Cyclin A2*, *Cyclin B1*, *Cyclin B2*, and *Cdc25c*, and the decrease of inhibitory genes, *e.g.*, *Cdkn1b* and *Cdk5rap1* (Fig. 6E). Interestingly, GO analysis showed that MAPK cascade ranked as the top one in the down-regulated signaling genes

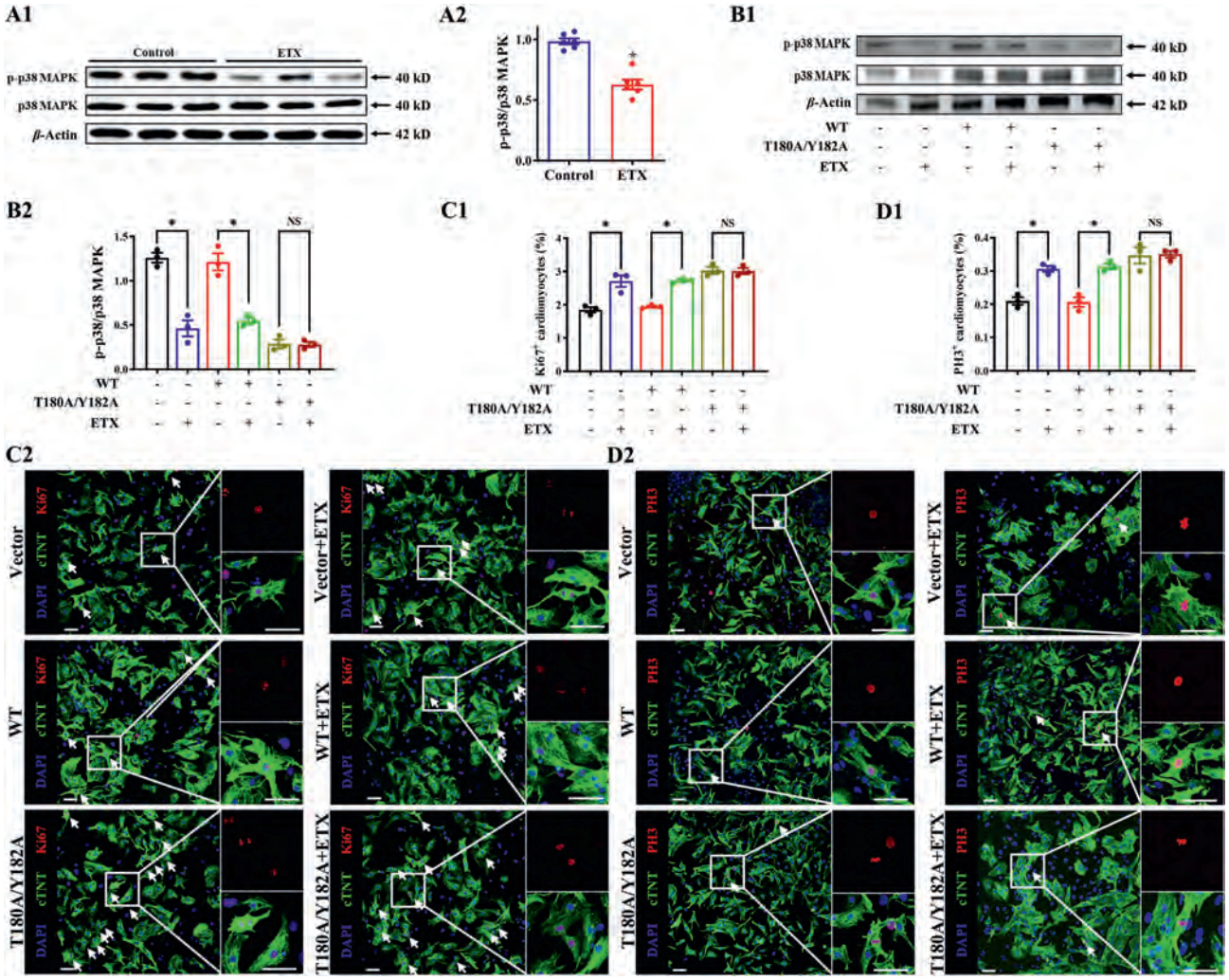

Figure 7 CPT1 inhibition induces cardiomyocytes proliferation *via* p38 MAPK signaling pathway in postnatal mice. (A) The effect of ETX treatment on p38 MPAK phosphorylation in P14 heats ($n = 6$, $^*P < 0.05$ *vs.* control). (B) The effect of ETX, p38 MAPK WT overexpression and p38 MAPK T180A/Y182A (T180A/Y182A) overexpression on p38 MPAK phosphorylation in P7 cardiomyocytes ($n = 3$, $^*P < 0.05$, NS＝Not significant). (C, D) The effect of ETX treatment, WT, and T180A/Y182A on the ratio of $Ki67^+$ (red, white arrow) or $PH3^+$ (red, white arrow) in P7 cardiomyocytes ($n = 3$, $^*P < 0.05$, NS＝Not significant). Scale bars = 50 μm. Error bars indicate SEM.

(Fig. 6B2). Therefore, we, next, analyzed the genes involved in MAPK signaling and found that 50 of the 102 genes were related to p38 MAPK signaling (Fig. 6F). This result indicated that p38 MAPK signaling may play the most important role in metabolic reprogramming-induced cardiomyocyte proliferation.

The key kinase of the MAPK signaling pathway, p38 MAPK, has been reported to regulate cardiomyocyte proliferation[12]. As shown in Fig. 7A, ETX significantly decreased p38 MAPK phosphorylation, while the expression of total p38 MAPK was unchanged. To verify the function of p38 MAPK phosphorylation in the ETX-induced cardiomyocyte proliferation, we used a phosphorylated mutant of p38 MAPK by replacing the threonine at 180 and tyrosine at 182 with the alanine (T180A/Y182A). We found that ETX could decrease p38 MAPK phosphorylation after p38 MAPK WT plasmid transduction, but the inhibitory function was abolished after p38 MAPK T180A/Y182A plasmid transduction (Fig. 7B). Besides, the pro-proliferative effect of ETX was also blocked in P7 cardiomyocytes after p38 MAPK T180A/Y182A plasmid transduction (Fig. 7C and D).

In addition to the *in vitro* experiments, we further studied the effect of p38 MAPK on adult cardiomyocytes *in vivo*, we generated AAV9 carrying *p38 Mapk-Flag* and *p38 Mapk* (T180A/Y182A)-*Flag* as an alternative to germline overexpression of *p38 Mapk-Flag* and *p38 Mapk* (T180A/Y182A). After MI, the negative control (vector) or AAV9 was immediately injected into the myocardium. We found that ETX could decrease p38 MAPK phosphorylation in *p38 Mapk* AAV9 group, but not in *p38 Mapk* (T180A/Y182A) AAV9 group (Fig. 8A). Consequently, the ETX-induced cardiomyocyte proliferation and improvement in cardiac function disappeared in *p38 Mapk* (T180A/Y182A) AAV9 group (Fig. 8B−E). These results further indicate that p38 MAPK signaling may play an important role in metabolic reprogramming-induced cardiomyocyte proliferation.

To explore how ETX inhibited p38 MAPK phosphorylation, the p38 MAPK-related kinases and phosphatases were investigated. We selected *Map2k3* as the representative of direct kinase, and *Dusp1*, *Dusp4*, and *Dusp12* as the representative phosphatases, because those enzymes were significantly different between

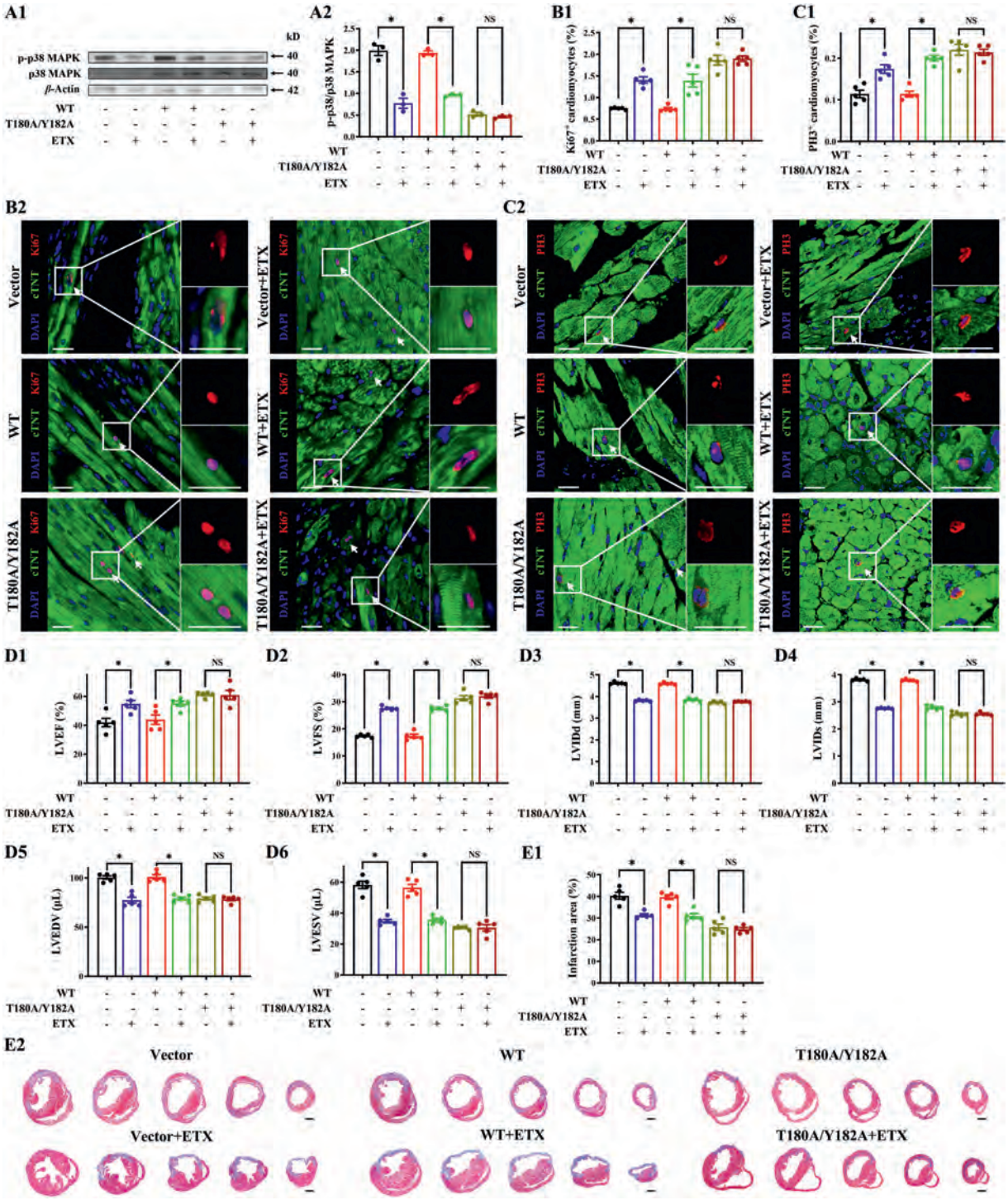

Figure 8 CPT1 inhibition induces cardiomyocytes proliferation *via* p38 MAPK signaling pathway in adult mice. (A) The effect of ETX, p38 MAPK WT overexpression and p38 MAPK T180A/Y182A (T180A/Y182A) overexpression on p38 MPAK phosphorylation in adult mice heart ($n = 3$, $^*P < 0.05$, NS = Not significant). (B, C) The effect of ETX treatment, WT, and T180A/Y182A on the ratio of $Ki67^+$ (red, white arrow) or $PH3^+$ (red, white arrow) cardiomyocytes in adult mice hearts ($n = 5$, $^*P < 0.05$, NS = Not significant; Scale bars = 20 μm). (D) LVEF, LVFS, LVIDd, LVIDs, LVEDV and LVESV at 4 weeks after MI were measured in mice after treatment with or without ETX, WT and T180A/Y182A ($n = 5$, $^*P < 0.05$, NS = Not significant). (E) The infarcted area of the heart in mice 4 weeks after MI treated with or without ETX, WT and T180A/Y182A ($n = 5$, $^*P < 0.05$, NS = Not significant; Scale bars = 1 mm). Error bars indicate SEM.

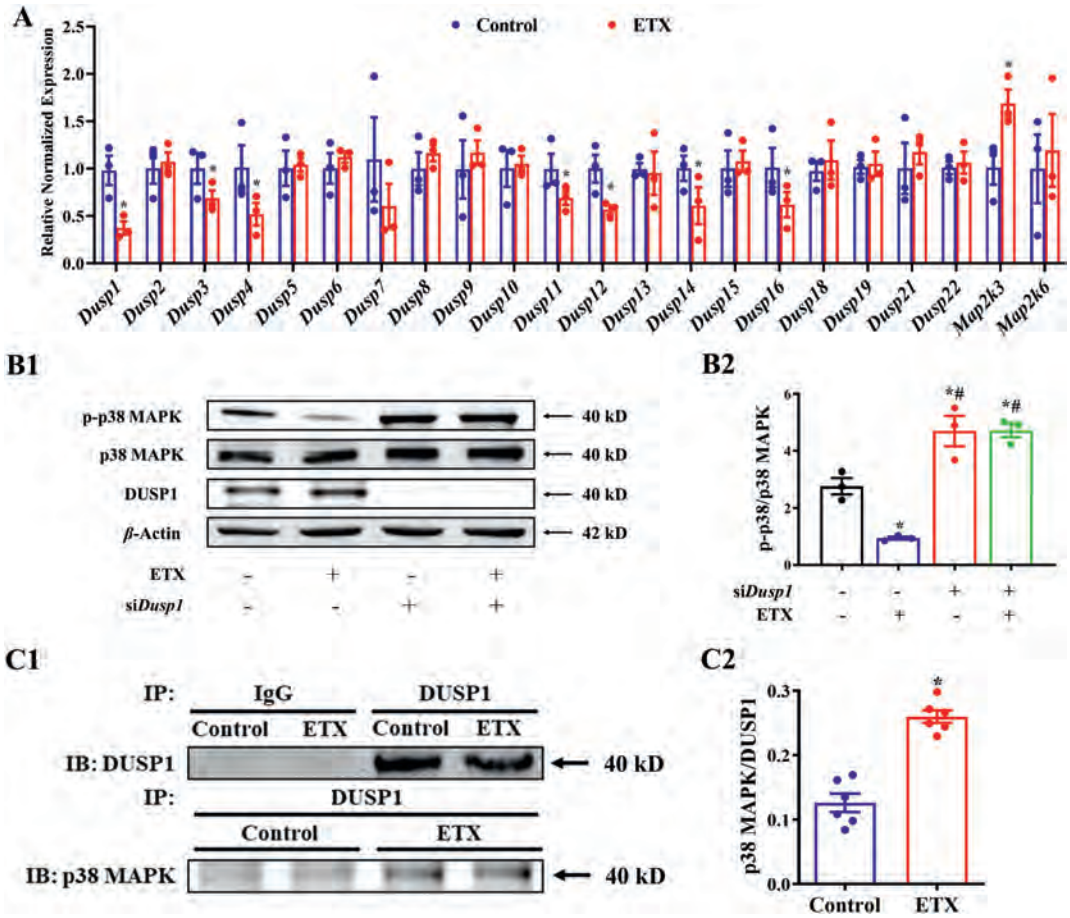

Figure 9 DUPS1 regulates p38 MAPK signaling after CPT1 inhibition in postnatal cardiomyocytes. (A) The expression of *Map2k3*, mitogen-activated protein kinase kinase 6 (*Map2k6*), and dual specificity phosphatase family (*Dusp1*, *Dusp2*, *Dusp3*, *Dusp4*, *Dusp5*, *Dusp6*, *Dusp7*, *Dusp8*, *Dusp9*, *Dusp10*, *Dusp11*, *Dusp12*, *Dusp13*, *Dusp14*, *Dusp15*, *Dusp16*, *Dusp18*, *Dusp19*, *Dusp21*, *Dusp22*) in P1 and P7 cardiomyocytes ($n = 6$, $^*P < 0.05$ *vs.* P1). (B) The effect of ETX treatment and *Dusp1* siRNA (si*Dusp1*) on DUSP1 expression and p38 MAPK phosphorylation in P7 cardiomyocytes ($n = 3$, $^*P < 0.05$ *vs.* Control, $^{\#}P < 0.05$ *vs.* ETX). (C) The effect of ETX treatment on the interaction of DUSP1 and p38 MAPK in P7 cardiomyocytes ($n = 6$, $^*P < 0.05$ *vs.* Control). Error bars indicate SEM.

P1 and P7 cardiomyocytes. The increase in *Map2k3* and decrease in *Dusp1*, *Dusp4*, and *Dusp12* were accompanied by an increase in p38 MAPK phosphorylation (Fig. 9A and Supporting Information Fig. S7A). Although ETX had no effect on *Dusp1* expression (Fig. S7B and S7C), down-regulation of DUSP1 by siRNA blocked the inhibitory effect of ETX on p38 MAPK phosphorylation (Fig. 9B), while other enzyme siRNAs did not have this blocking effect (Fig. S7D−S7F), indicating that DUSP1 was involved in the inhibition of p38 MAPK phosphorylation by ETX. Further experiments showed the linkage between p38 MAPK and DUSP1, determined by co-immunoprecipitation, which was increased by ETX treatment, implying that ETX induced the decrease in p38 MAPK phosphorylation *via* DUSP1 (Fig. 9C).

3.5. CPT1 inhibition suppressed p38 MAPK phosphorylation mediated by ADP-ribosylation of DUSP1

Metabolic reprogramming should induce a holistic change of metabolites in cardiomyocytes and stimulate cardiomyocyte proliferation. To investigate whether metabolites could regulate the interaction of p38 MAPK and DUSP1, untargeted metabolomics was used to analyze the different metabolites after ETX treatment. ETX was injected daily for 1 week in P7 mice and the hearts were harvested at P14 for metabolomics studies. Unsupervised analysis of metabolite levels demonstrated a significant effect of ETX on cardiomyocyte metabolome (Fig. 10A, Supporting Information Fig. S8A and Table S1). It identified 68 up-regulated and 120 down-regulated metabolites in ETX-treated hearts, in which many of the metabolites are associated with FAO and tricarboxylic acid cycle, such as palmitoleic acid, carnitine, malic acid, and propionylcarnitine. As shown in Fig. 10B, among the 188 different metabolites, a protein post-translational modification molecule ADP-ribose changed the most after ETX treatment (8.2-fold increase), indicating that ADP-ribosylation may play an important role in the pathophysiological process, due to the negative relationship between free ADP-ribose and ADP-ribosylation[18]. Untargeted metabolomics results revealed an increase in free ADP-ribose in ETX-treated P7 cardiomyocytes while ADP-ribosylation of protein was decreased after ETX treatment determined by Western blots (Fig. 10B and C). These indicate that there was an increase in free ADP-ribose, accompanied by a decrease in ADP-ribosylation in ETX-treated P7 cardiomyocytes. ADP-ribosylation is regulated by several enzymes, including ADP-ribosyltransferases (ARTs), poly(ADP-ribose) polymerases (PARPs), and ADP-ribosyl

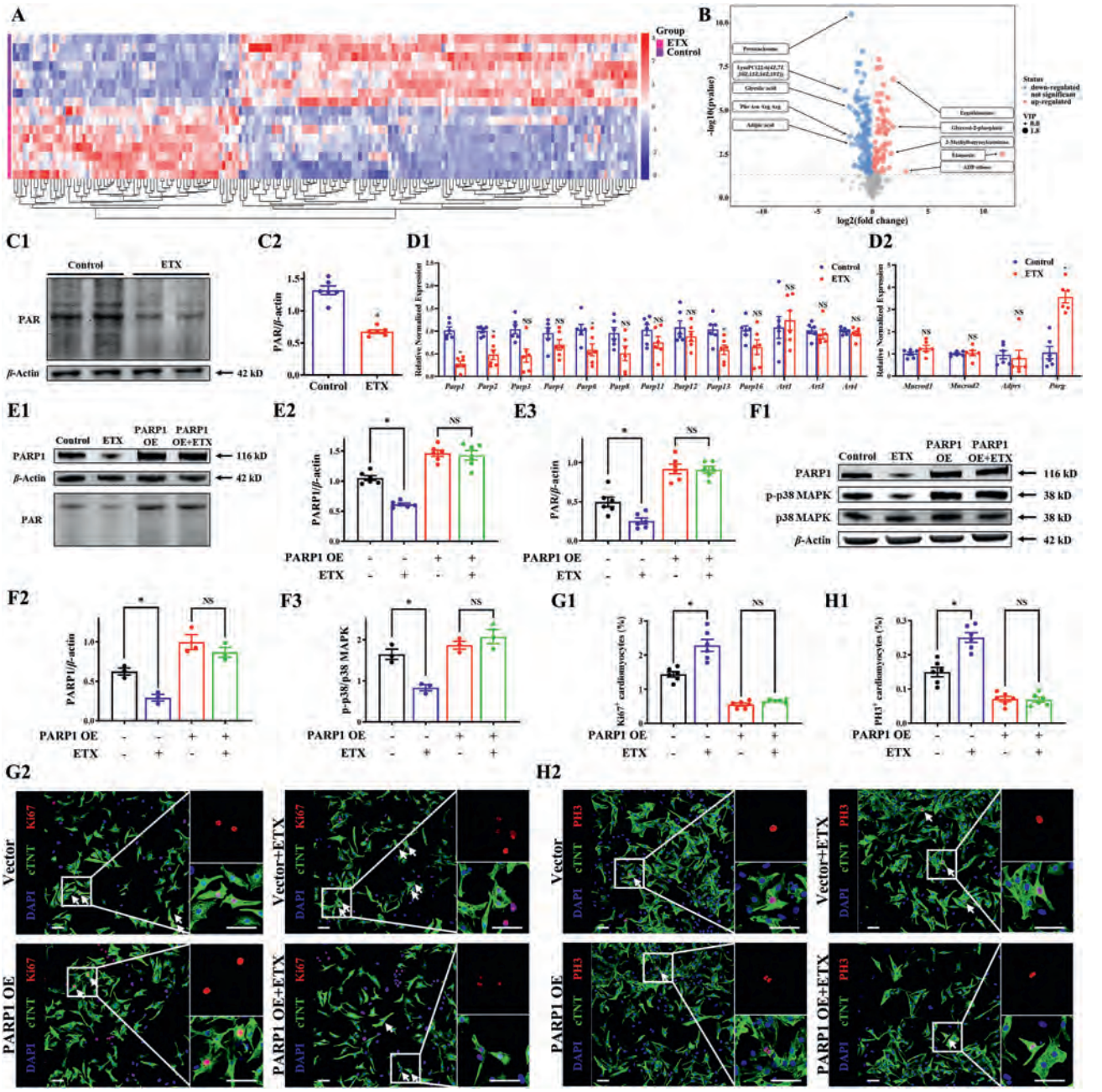

Figure 10 CPT1 inhibition suppresses p38 MAPK phosphorylation mediated by PARP1 regulated ADP-ribosylation. (A) The relative abundance of metabolites extracted from octuplicate samples of control and ETX-treated heart ($n = 8$). (B) Volcano plot for the control and ETX-treated hearts and the top 5 metabolites in up or down-regulated metabolites are shown ($n = 8$). (C) The effect of ETX on poly(ADP-ribose) (PAR) protein in P7 cardiomyocytes determined by immunoblotting ($n = 6$, $^*P < 0.05$ *vs.* Control). (D) *Parp1*, poly(ADP-ribose) polymerase 2 (*Parp2*), poly(ADP-ribose) polymerase 3 (*Parp3*), poly(ADP-ribose) polymerase 4 (*Parp4*), poly(ADP-ribose) polymerase 6 (*Parp6*), poly(ADP-ribose) polymerase 8 (*Parp8*), poly(ADP-ribose) polymerase 11 (*Parp11*), poly(ADP-ribose) polymerase 12 (*Parp12*), poly(ADP-ribose) polymerase 13 (*Parp13*), poly(ADP-ribose) polymerase 16 (*Parp16*), ADP-ribosyltransferase 1 (*Art1*), ADP-ribosyltransferase 3 (*Art3*), ADP-ribosyltransferase 4 (*Art4*), mono-ADP ribosylhydrolase 1 (*Macrod1*), mono-ADP ribosylhydrolase 2 (*Macrod2*), ADP-ribosylserine hydrolase (*Adprs*), and poly(ADP-ribose) glycohydrolase (*Parg*) gene expression with ETX or without (Control) ETX treatment in P7 cardiomyocytes ($n = 6$, $^*P < 0.05$ *vs.* Control). (E) The effect of ETX treatment and PARP1 overexpression (PARP1 OE) on PARP1 and PAR expression in P7 cardiomyocytes ($n = 6$, $^*P < 0.05$, NS = Not significant). (F) The effect of ETX treatment and/or PARP1 OE on PARP1 expression and p38 MPAK phosphorylation in P7 cardiomyocytes ($n = 3$, $^*P < 0.05$, NS = Not significant). (G, H) The effect of ETX treatment and PARP1 OE on the ratio of $Ki67^+$ (red, white arrow) or $PH3^+$ (red, white arrow) in P7 cardiomyocytes ($n = 6$, $^*P < 0.05$, NS = Not significant; Scale bars = 50 μm). Error bars indicate SEM.

hydrolases (PARG, ADRPS and MACORDs). Our additional study showed that, although ETX treatment led to changes in the expression of several enzymes, the decrease in *Parp1* expression was the biggest (Fig. 10D). PARP1 expression was also decreased both in *Cpt1a*$^{-/-}$ and *Cpt1b*$^{-/-}$ mice hearts (Fig. S8B). PARP1 overexpression blocked the inhibitory effect of ETX on ADP-ribosylation and p38 MAPK phosphorylation in cardiomyocytes (Fig. 10E and F), accompanied by blockade of ETX-induced cardiomyocyte proliferation (Fig. 10G and H), indicating the key role of PARP1 in the ETX-mediated signal pathway.

As stated above, DUSP1 is involved in the ETX-induced decrease in p38 MAPK phosphorylation, we wondered whether ADP-ribosylation affects DUSP1 function and is involved in ETX-mediated decrease in p38 MAPK phosphorylation. Co-immunoprecipitation experiment showed the linkage between PARP1 and DUSP1, which was decreased by ETX treatment (Fig. 11A), accompanied with decreased ADP-ribosylation of DUSP1 after ETX treatment (Fig. 11B). The involvement of *Parp1* was further confirmed by a mutation study. We used a catalytic mutant of *Parp1* by replacing the glutamic acid at 988 with a lysine (E988K) which had no poly(ADP-ribose) polymerase activity, determined by the following experiments. The overexpression of WT PARP1 in cardiomyocytes increased the ADP-ribosylation of DUSP1, decreased the interaction of DUSP1 and p38 MAPK and led to the increase in p38 MAPK phosphorylation. However, E988K had no effect on the ADP-ribosylation of DUSP1, the interaction of DUSP1 and p38 MAPK, and p38 MAPK phosphorylation (Fig. S8C and S8D). Moreover, PARP1 WT overexpression blocked the inhibitory effect of ETX on DUSP1 ADP-ribosylation and the interaction of DUSP1 and p38 MAPK (Fig. 11C). Taken together, these results further indicate that the regulation of DUSP1 and p38 MAPK binding was dependent on ADP-ribosylation, mediated by PARP1. ETX, by decreasing PARP1, negatively regulated ADP-ribosylation modification of DUSP1, and therefore, negatively affected p38 MAPK phosphorylation and function.

To study further the effect of PARP1 on cardiomyocytes, we generated AAV9 carrying *Parp1-Flag* as an alternative to germline overexpression of *Parp1*. After ligation of the LAD coronary artery of MADM mice, the negative control (vector) or *Parp1-Flag* AAV9 was immediately injected into the myocardium. We found that the ability of ETX to ameliorate cardiac function (Fig. 11D and Fig. S8E) and decrease infarct size (Fig. 11E) were blocked by *Parp1* overexpression. In addition, we found that ETX-induced cardiomyocyte proliferation, assessed by single-colored green or red cardiomyocytes in MADM mice, was blocked by *Parp1* overexpression (Fig. 11F). We also noticed that *Parp1* overexpression blocked the effect of ETX on DUSP1 ADP-ribosylation and the interaction of DUSP1 and p38 MAPK, and therefore, blocked the effect of ETX on p38 MAPK phosphorylation in mice hearts (Fig. 11G and Fig. S8F). Collectively, this study suggested that CPT1 inhibition may negatively regulate ADP-ribosylation of DUSP1 through PARP1, decreasing the phosphorylation but increasing the function of p38 MAPK, resulting in an increase in cardiomyocyte proliferation (Fig. 12).

4. Discussion

In our study, we found that *Cpt1a* or *Cpt1b* conditional cardiomyocyte-specific knockout ameliorated the pathological effects of MI by promoting cardiomyocyte proliferation. Similar effects were also observed in mice treated with ETX after MI, which might be a new and potential therapeutic approach.

In the mammalian heart, dramatic maturational changes in energy metabolism occur in the newborn period, shifting from glycolysis to FAO[19]. This shift mainly occurs during the first postnatal week and coincides with the sharp loss of cardiac regenerative capacity. Our data show that inhibiting glycolysis on the P1 heart by targeting enzyme GCK decreased cardiomyocyte proliferation. By contrast, inhibiting FAO by targeting CPT1 enzymes on P7 heart increased cardiomyocyte proliferation. Manipulation of these enzymes effectively induces metabolic reprogramming. Therefore, our findings support the idea that interfering with metabolic reprogramming is an effective strategy to manipulate cardiac regeneration and repair.

In our experiments, CPT1 ranked at the top of the FAO enzymes that had an increase in mRNA expression in the postnatal heart. CPT1 is located at the outer surface of the mitochondrial membrane, controlling the mitochondrial uptake of long-chain acyl-CoAs and catalyzing the transfer of the acyl group from coenzyme A to carnitine to form palmitoylcarnitine[20]. Either genetic cardiac-specific CPT1 deletion or mitochondrial CPT1 inhibition with ETX was sufficient to partially reverse the metabolic reprogramming. CPT1 is the first rate-limiting enzyme and a major mechanism regulating mitochondrial FAO[15]. To determine the effect of CPT1 inhibition on cardiomyocyte proliferation, a variety of techniques to identify nuclear and cell division were used to confirm our findings. It is known that both Ki67 and PH3 can estimate the proliferative capacity of cells, which is widely used to investigate cell cycle activity and cell proliferation. However, in cardiomyocytes, the reentry into the cell cycle could cause nuclear division rather than cell division in the setting of cardiomyocyte polyploidy, as well as multinuclearity. Therefore, Ki67 and PH3, as markers, could overestimate the extent of cardiomyocyte proliferation. Given this possibility, MADM mice and time-lapse imaging microscopy were used to confirm our findings, which could directly observe cardiomyocyte division at the single-cell level, although MADM may underestimate the extent of cardiomyocyte proliferation[10,21]. The total number of cardiomyocytes in hearts was counted in our study to confirm the proproliferative effect of ETX on cardiomyocytes.

Numerous studies have investigated the protective effect of CPT1 on cardiac function. Inactivating CPT1 improved lipid overload-induced mitochondrial dysfunction and cardiac hypertrophy[22]. CPT1 inhibition in infant mice delayed cardiomyocyte cell cycle exit, hypertrophic growth, and maturation[7]. A recent study showed that partial deletion of carnitine palmitoyltransferase 2, another enzyme essential for beta-oxidation of long-chain fatty acids in the mitochondria, enhanced cardiomyocyte proliferation without an increase in heart size[23]. These reports indicated that CPT1 inhibition can protect the heart from injury and induce cardiac regeneration. Our study not only demonstrated that CPT1 inhibition delayed the cell cycle arrest in neonatal mice, but also showed that the 4-OH-tamoxifen-inducible, cardiac-specific deletion of *Cpt1a* and *Cpt1b* improved cardiomyocyte proliferation and cardiac function post-MI in adult mice. A correct duration of CPT1 inhibition may be a treatment strategy with clinical significance. CPT1 has been recognized as a treatment target for metabolic therapies aimed to improve cardiac performance in patients with heart failure[16]. Specific CPT1 inhibitors, such as ETX, have been actively pursued as therapeutic agents[17]. ETX can switch energy metabolism from fatty acids to glucose oxidation in the adult heart[17]. Animal studies and initial clinical trials in humans supported the ETX's therapeutic effect against heart failure[24].

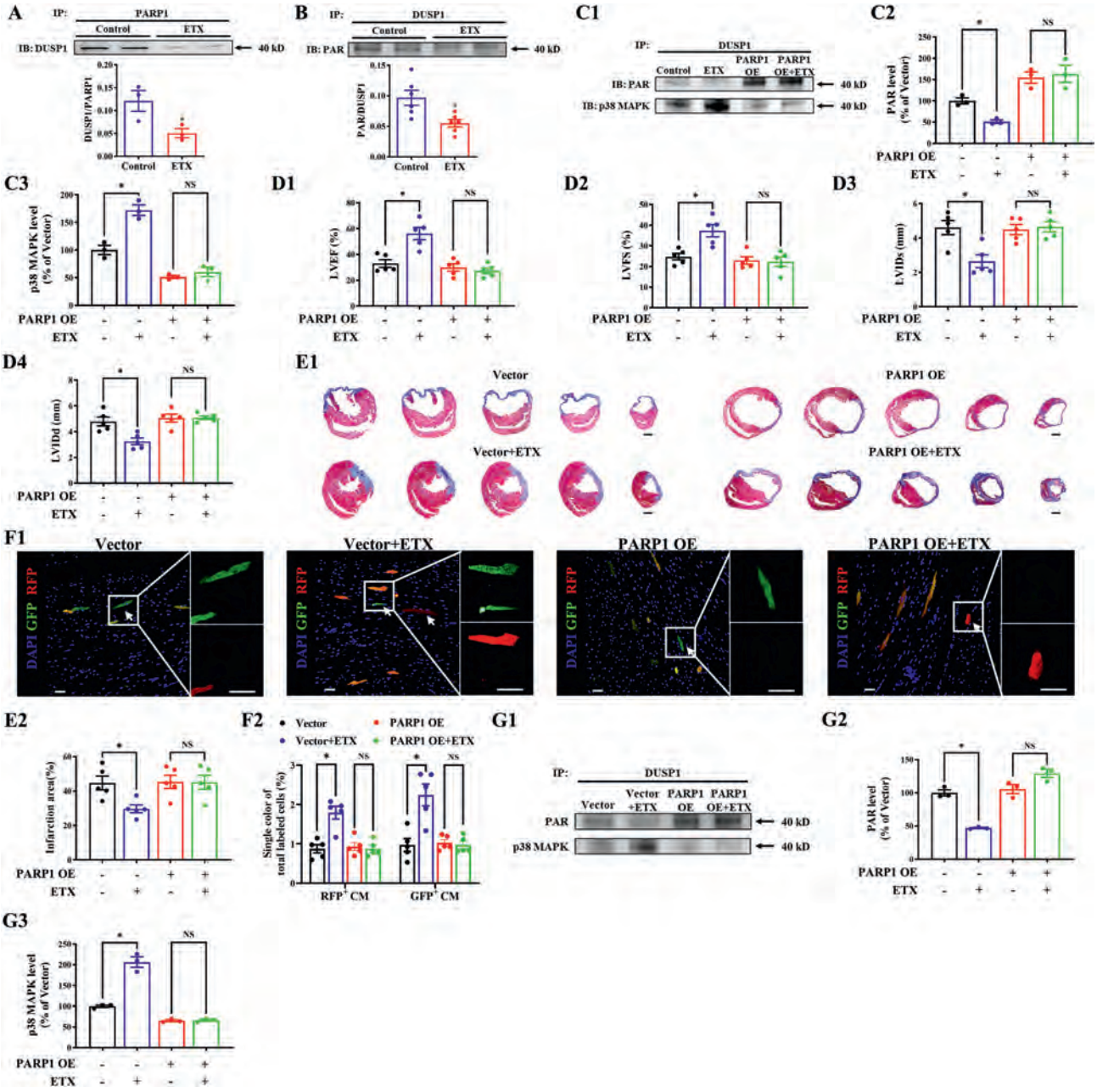

Figure 11 CPT1 inhibition suppresses p38 MAPK phosphorylation mediated by ADP-ribosylation of DUSP1. (A) The effect of ETX treatment on the interaction between DUSP1 and PARP1 in P7 cardiomyocytes ($n = 4$, $^*P < 0.05$ *vs.* Control). (B) The effect of ETX treatment on the on ADP-ribosylation of DUSP1 in P7 cardiomyocytes ($n = 4$, $^*P < 0.05$ *vs.* Control). (C) The effect of ETX treatment and/or PARP1 OE on ADP-ribosylation of DUSP1 and the interaction between DUSP1 and p38 MAPK in P7 cardiomyocytes ($n = 3$, $^*P < 0.05$, NS = Not significant). (D) LVEF, LVFS, LVIDd and LVIDs at 4 weeks after MI were measured in MADM mice after treatment with ETX and/or PARP1 AAV9 (PARP1 overexpression, PARP1 OE) ($n = 5$, $^*P < 0.05$, NS = Not significant). (E) The infarcted area of the heart in mice 4 weeks after MI treated with control (Vector), ETX, and/or PARP1 OE ($n = 5$, $^*P < 0.05$, NS = Not significant; Scale bars = 1 mm). (F) Representative immunofluorescence and quantification of single-labeled (red or green, white arrow) cardiomyocytes in MADM mice after MI for 4 weeks treated with control (Vector), ETX, and/or PARP1 OE ($n = 5$, $^*P < 0.05$, NS = Not significant; Scale bars = 20 μm). (G) The effect of ETX and PARP1 OE on ADP-ribosylation of DUSP1 and the interaction between DUSP1 and p38 MAPK in mice hearts ($n = 3$, $^*P < 0.05$, NS = Not significant). Error bars indicate SEM.

Recent studies investigated the mechanism of metabolic reprogramming-induced cardiomyocyte proliferation. Loss of pyruvate dehydrogenase kinase 4 increased glucose oxidation relative to fatty-acid oxidation, consequently increasing cardiomyocyte proliferation by decreasing DNA damage and expression of DNA-damage response markers[25]. The increase in the expression of pyruvate kinase muscle isoenzyme 2, an isoenzyme of pyruvate kinase, promoted cardiomyocyte proliferation which was mediated by reducing ROS production, oxidative DNA damage, and upregulating the β-catenin signaling pathway[8].

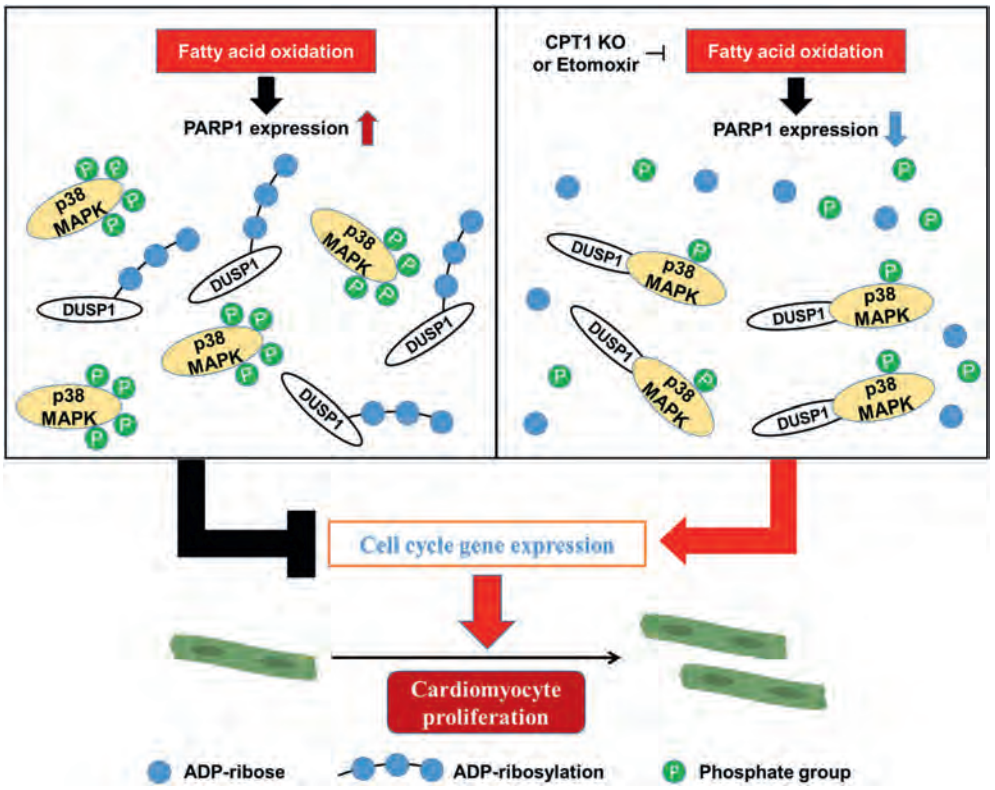

Figure 12 Schematic representation of the proposed effect of reversing metabolic reprogramming by CPT1 inhibition on cardiomyocyte proliferation and heart regeneration. Inhibition of FAO by CPT1 KO or Etomoxir decreases PARP1 expression, negatively regulates ADP-ribosylation modification of DUSP1 and dephosphorylates p38 MAPK which increases cell cycle gene expression and promotes cardiomyocyte proliferation. The suppression of postnatal cardiomyocyte cell-cycle arrest increases cardiac regeneration post myocardial infraction injury.

Malonate, which contributes to a metabolic shift into glycolytic metabolism, promotes adult cardiomyocyte proliferation and heart regeneration by decreasing DNA damage[14]. FAO inhibition by deleting *Cpt1b* could promote cardiomyocyte proliferation through increasing α-ketoglutarate (α-KG) production and α-KG activated lysine demethylase 5 (KDM5) expression. However, whether α-KG itself or KDM5 activation could induce cardiomyocyte proliferation *in vivo* was not mentioned in this study[9]. Besides, KDM5 expression was absent in adult hearts. Thus, α-KG or KDM5 activators alone may not be enough to explain the effect of FAO deletion on cardiac regeneration in adult hearts[26]. In our study, we used mRNA microarray analysis to investigate the effect of ETX treatment on cardiomyocyte gene expression. According to the pathway analysis, the MAPK signaling pathway was ranked at the top of significantly altered pathways. Further analysis of the differentially expressed genes of the MAPK signaling pathway showed that the majority of genes were related to the p38 MAPK pathway. The p38 MAPK pathway has been reported to be associated with cardiomyocyte proliferation. Inhibiting p38 MAPK alone could promote cardiomyocyte proliferation, through a mechanism that involves enhancing Cyclin D2 and/or Cyclin A2 expression[27]. Our data suggested that p38 MAPK inhibition may mediate the ETX-induced pro-proliferative effect. Our results further indicated that p38 MAPK inhibition was regulated by dephosphorylation of DUSP1. Metabolic reprogramming could promote the binding of p38 MAPK and DUSP1.

There are pieces of evidence, including a genetic study, showing the effect of p38 MAPK on cardiomyocyte proliferation. For example, cardiac-specific p38 MAPK alpha knockout mice have a 92.3% increase in neonatal cardiomyocyte mitoses and the inhibition of p38 MAPK in adult cardiomyocytes promotes cytokinesis[28]. Moreover, the inhibition of p38 MAPK phosphorylation increased cardiomyocyte proliferation[27]. Active p38 *M*APK but not dominant negative p38 *M*APK blocked the proliferation of adult zebrafish cardiomyocytes and heart regeneration[29]. The overexpression of miR-708 promoted cardiomyocyte proliferation through inhibition of p38 MAPK expression[30]. Connexin43 knockdown promoted the proliferation of neonatal cardiomyocytes by the combined inactivation of p38 MAPK and increased expression of FGF1[31]. FAK-related nonkinase expression reduced cardiomyocyte proliferation by inducing p38 MAPK activation and cell cycle withdrawal[32]. In addition to the p38-mediated cardiomyocyte proliferation, there are also reports showing that activation of p38 MAPK can induce cardiac hypertrophy[33-35]. Overall, the aforementioned studies, using molecular biological methods, including genetics, show the role of p38 MAPK on cardiomyocyte regeneration. However, cardiomyocyte proliferation was not analyzed in these studies and therefore the pro-proliferative effect of p38 MAPK in the heart was not reported.

As a kinase, p38 MAPK has many downstream signaling genes; some genes cause cell hypertrophy (*e.g.*, transforming growth factor-β, DEP domain containing MTOR-interacting protein (DEPTOR), cAMP response element-binding protein (CREB)) while other genes (*e.g.*, inositol requiring enzyme 1 alpha (IRE1α)/X-box binding protein 1 (XBP1)) are involved in cell proliferation, although the reasons leading to the different signaling pathways are not known. For example, regarding hypertrophy, inhibition of p38 signaling reduced

transforming growth factor-β signaling-related hypertrophic gene expression and blocked the exaggerated cardiac remodeling in cardiomyocytes[33]. The p38γ/δ promotes cardiac hypertrophy by phosphorylating DEPTOR, a mTORC1/mTORC2 inhibitor, which leads to DEPTOR degradation and mTOR activation[34]. It has been found that C1q-TNF-related protein-3 attenuates pressure overload-induced cardiac hypertrophy by suppressing the p38 MAPK/CREB pathway[35]. Regarding cell proliferation, it was reported that inhibition of p38 MAPK phosphorylation increased cardiomyocyte proliferation, *via* up-regulation of cell cycle genes, including Cyclin A2, *Cdc2a*, and Cyclin B[27,28]. Other reports showed that the inhibition of p38 MAPK phosphorylation increased cardiomyocyte proliferation *via* IRE1α/XBP1-mediated gene regulation. p38 MAPK inactivation induces XBP1 activity *via* IRE1α-mediated posttranscriptional splicing and nuclear translocation[36]. Although the reasons leading to the discrepant consequences mediated by p38 MAPK are not clear, differences in downstream signaling could partially cause the duality of p38 MAPK in the heart.

Based on the above results, we speculated that metabolic reprogramming may promote cardiomyocyte proliferation through inhibition of DUSP1−p38 MAPK and its downstream pathways. However, it was still unclear how metabolic reprogramming induces cardiomyocyte proliferation through regulation of the linkage of p38 MAPK and DUSP1. Untargeted metabolomics was used to analyze the different metabolites after ETX treatment. We found that ADP-ribosylation was involved in metabolic reprogramming induction of cardiomyocyte proliferation. ADP-ribosylation has been reported to play an important role in DNA repair[37]. ROS are mainly produced by FAO in adult hearts, which induce DNA damage and genomic instability[38]. ADP-ribosylation mediated by PARPs is a protective mechanism that could alleviate DNA damage by modifying histone or DNA damage-response-related proteins. In the current study, we found that PARP1 was the main enzyme that blocked ADP-ribosylation of proteins in cardiomyocytes after ETX treatment. Therefore, we speculated that ADP-ribosylation could affect the binding of p38 MAPK and DUSP1. In this study, we first demonstrated that ADP-ribosylation is involved in regulating p38 MAPK phosphorylation. We demonstrated that DUSP1 can be ADP-ribosylated by PARP1, which could affect the binding between DUSP1 and p38 MAPK. ADP-ribosylation of DUSP1 was decreased and the interaction of DUSP1 and p38 MAPK was increased after ETX treatment, which resulted in the dephosphorylation of p38 MAPK. Our findings were sufficient to explain the mechanism of metabolic reprogramming-regulated p38 MAPK phosphorylation. Other essential functions of ADP-ribosylation in post-transcriptional modification have been reported in several studies. It was reported that ADP-ribosylation persisted on chromatin throughout the cell cycle and affected transcription histone marks[39]. Ribosome ADP-ribosylation can inhibit translation and promote protein homeostasis[40]. ADP-ribosylation of activating transcription factor 4 can inhibit activating transcription factor 4 bound to DUSP1 promotor and decrease the transcription of DUSP1[41].

How ETX affects PARP1 function related to cardiomyocyte proliferation is still unsolved. Because of the difference between glycolysis and fatty oxidation in ROS production[42] and the damaging effect of ROS on DNA, we wondered whether ROS and DNA damage may be involved in the regulation of ETX on PARP1 expression. ADP-ribosylation mediated by PARPs is a protective mechanism that could mitigate DNA damage by modifying histone or DNA damage-response-related proteins[37]. It is possible that inhibition of FAO would decrease ROS and therefore, ROS-mediated DNA damage. In this situation, PARP1 would no longer be needed to repair DNA damage. Therefore, ETX treatment would lower PARP1 expression, although the detailed mechanism leading to the regulation of PARP1 is not completely known, which needs to be determined in the future.

Limitations of this study: As indicated, due to the limitation of Ki67 and PH3 as proliferative marker, we used C57BL/6J mice to count the total number of cardiomyocytes in hearts with or without ETX treatment. We also realized that, to further show the effect of CPT1 inhibition on cardiomyocyte proliferation, *Cpt1a*$^{-/-}$ and *Cpt1b*$^{-/-}$ mice should be used in the future.

5. Conclusions

Our study demonstrated that metabolic reprogramming from glycolysis to FAO contributes to the loss of cardiac regeneration capacity in neonatal mice, and reversal of the switch in the adult heart stimulates cardiac regeneration. Inhibition of FAO by targeting CPT1 is a potential therapeutic strategy for stimulating cardiomyocyte proliferation and protection of the heart from MI injury. CPT1 inhibition induced cardiomyocyte proliferation through a p38 MAPK-dependent mechanism which was mediated by ADP-ribosylation of DUSP1 *via* PARP1.

Acknowledgments

This study was supported by grants from the National Key Research and Development Program of China (No. 2022YFA1104500), National Natural Science Foundation of China (No. 81930008), Natural Science Foundation of Sichuan Province (No. 2023NSFSC1651, China), and the National Institutes of Health (No. DK134574 and No. DK119652, US).

Author contributions

Luxun Tang: Writing − review & editing, Writing − original draft, Project administration, Methodology, Investigation, Formal analysis, Data curation, Conceptualization. Yu Shi: Project administration, Methodology, Investigation, Formal analysis, Data curation. Qiao Liao: Project administration, Methodology, Investigation, Formal analysis, Data curation. Feng Wang: Project administration, Methodology, Investigation. Hao Wu: Project administration, Methodology, Investigation. Hongmei Ren: Project administration, Methodology, Investigation. Xuemei Wang: Project administration, Methodology, Investigation. Wenbin Fu: Project administration, Methodology, Investigation. Jialing Shou: Project administration, Methodology, Investigation. Wei Eric Wang: Validation, Supervision, Conceptualization. Pedro A. Jose: Writing − review & editing, Validation, Supervision, Resources, Funding acquisition. Yongjian Yang: Writing − review & editing, Validation, Supervision, Resources, Conceptualization. Chunyu Zeng: Writing − review & editing, Writing − original draft, Validation, Supervision, Resources, Funding acquisition, Conceptualization.

Conflicts of interest

The authors declare no conflicts of interest.

Appendix A. Supporting information

Supporting information to this article can be found online at https://doi.org/10.1016/j.apsb.2024.11.001.

References

1. Prasad V, Molkentin JD. At the brink of human therapy to generate new myocytes in the adult injured heart. *Circulation* 2022;**145**: 1356−8.
2. Mohamed TM, Ang YS, Radzinsky E, Zhou P, Huang Y, Elfenbein A, et al. Regulation of cell cycle to stimulate adult cardiomyocyte proliferation and cardiac regeneration. *Cell* 2018;**173**:104−16.e12.
3. Du J, Zheng L, Gao P, Yang H, Yang WJ, Guo F, et al. A small-molecule cocktail promotes mammalian cardiomyocyte proliferation and heart regeneration. *Cell Stem Cell* 2022;**29**:545−58.e13.
4. Du D, Liu C, Qin M, Zhang X, Xi T, Yuan S, et al. Metabolic dysregulation and emerging therapeutical targets for hepatocellular carcinoma. *Acta Pharm Sin B* 2022;**12**:558−80.
5. Ryall JG, Dell'Orso S, Derfoul A, Juan A, Zare H, Feng X, et al. The NAD^+-dependent SIRT1 deacetylase translates a metabolic switch into regulatory epigenetics in skeletal muscle stem cells. *Cell Stem Cell* 2015;**16**:171−83.
6. Lopaschuk GD, Jaswal JS. Energy metabolic phenotype of the cardiomyocyte during development, differentiation, and postnatal maturation. *J Cardiovasc Pharmacol* 2010;**56**:130−40.
7. Cao T, Liccardo D, LaCanna R, Zhang X, Lu R, Finck BN, et al. Fatty acid oxidation promotes cardiomyocyte proliferation rate but does not change cardiomyocyte number in infant mice. *Front Cel Dev Biol* 2019;**7**:42.
8. Magadum A, Singh N, Kurian AA, Munir I, Mehmood T, Brown K, et al. Pkm2 regulates cardiomyocyte cell cycle and promotes cardiac regeneration. *Circulation* 2020;**141**:1249−65.
9. Li X, Wu F, Günther S, Looso M, Kuenne C, Zhang T, et al. Inhibition of fatty acid oxidation enables heart regeneration in adult mice. *Nature* 2023;**622**:619−26.
10. Wang WE, Li L, Xia X, Fu W, Liao Q, Lan C, et al. Dedifferentiation, proliferation, and redifferentiation of adult mammalian cardiomyocytes after ischemic injury. *Circulation* 2017;**136**:834−48.
11. Nabben M, van Bree BWJ, Lenaers E, Hoeks J, Hesselink MKC, Schaart G, et al. Lack of UCP3 does not affect skeletal muscle mitochondrial function under lipid-challenged conditions, but leads to sudden cardiac death. *Basic Res Cardiol* 2014;**109**:447.
12. Li Y, Xiong Z, Yan W, Gao E, Cheng H, Wu G, et al. Branched chain amino acids exacerbate myocardial ischemia/reperfusion vulnerability *via* enhancing GCN2/ATF6/PPAR-α pathway-dependent fatty acid oxidation. *Theranostics* 2020;**10**:5623−40.
13. Wang X, Li X, Liu S, Brickell AN, Zhang J, Wu Z, et al. PCSK9 regulates pyroptosis *via* mtDNA damage in chronic myocardial ischemia. *Basic Res Cardiol* 2020;**115**:66.
14. Bae J, Salamon RJ, Brandt EB, Paltzer WG, Zhang Z, Britt EC, et al. Malonate promotes adult cardiomyocyte proliferation and heart regeneration. *Circulation* 2021;**143**:1973−86.
15. van Weeghel M, Abdurrachim D, Nederlof R, Argmann CA, Houtkooper RH, Hagen J, et al. Increased cardiac fatty acid oxidation in a mouse model with decreased malonyl-CoA sensitivity of CPT1B. *Cardiovasc Res* 2018;**114**:1324−34.
16. Doenst T, Nguyen TD, Abel ED. Cardiac metabolism in heart failure: implications beyond ATP production. *Circ Res* 2013;**113**:709−24.
17. Schmidt-Schweda S, Holubarsch C. First clinical trial with etomoxir in patients with chronic congestive heart failure. *Clin Sci (Lond)* 2000; **99**:27−35.
18. Bort A, G Sánchez B, León C, Nozal L, Mora-Rodríguez JM, Castro F, et al. Metabolic fingerprinting of chemotherapy-resistant prostate cancer stem cells. An untargeted metabolomic approach by liquid chromatography−mass spectrometry. *Front Cel Dev Biol* 2022;**10**: 1005675.
19. Fukushima A, Alrob OA, Zhang L, Wagg CS, Altamimi T, Rawat S, et al. Acetylation and succinylation contribute to maturational alterations in energy metabolism in the newborn heart. *Am J Physiol Heart Circ Physiol* 2016;**311**:H347−63.
20. He L, Kim T, Long Q, Liu J, Wang P, Zhou Y, et al. Carnitine palmitoyltransferase-1b deficiency aggravates pressure overload-induced cardiac hypertrophy caused by lipotoxicity. *Circulation* 2012;**126**:1705−16.
21. Yerushalmi R, Woods R, Ravdin PM, Hayes MM, Gelmon KA. Ki67 in breast cancer: prognostic and predictive potential. *Lancet Oncol* 2010;**11**:174−83.
22. Zheng P, Wu H, Gu Y, Li L, Hu R, Ma W, et al. Atorvastatin ameliorates lipid overload-induced mitochondrial dysfunction and myocardial hypertrophy by decreasing fatty acid oxidation through inactivation of the p-STAT3/CPT1 pathway. *Biomed Pharmacother* 2023;**157**:114024.
23. Hirose K, Payumo AY, Cutie S, Hoang A, Zhang H, Guyot R, et al. Evidence for hormonal control of heart regenerative capacity during endothermy acquisition. *Science* 2019;**364**:184−8.
24. Heggermont WA, Papageorgiou AP, Heymans S, van Bilsen M. Metabolic support for the heart: complementary therapy for heart failure? *Eur J Heart Fail* 2016;**18**:1420−9.
25. Cardoso AC, Lam NT, Savla JJ, Nakada Y, Pereira AHM, Elnwasany A, et al. Mitochondrial substrate utilization regulates cardiomyocyte cell cycle progression. *Nat Metab* 2020;**2**:167−78.
26. Tang X. Regenerating the heart by metabolically reprogramming the cardiomyocyte epigenome. *Cell Metab* 2023;**35**:1849−51.
27. Engel FB, Hsieh PC, Lee RT, Keating MT. FGF1/p38 MAP kinase inhibitor therapy induces cardiomyocyte mitosis, reduces scarring, and rescues function after myocardial infarction. *Proc Natl Acad Sci U S A* 2006;**103**:15546−51.
28. Engel FB, Schebesta M, Duong MT, Lu G, Ren S, Madwed JB, et al. p38 MAP kinase inhibition enables proliferation of adult mammalian cardiomyocytes. *Genes Dev* 2005;**19**:1175−87.
29. Jopling C, Suñe G, Morera C, Izpisua Belmonte JC. p38α MAPK regulates myocardial regeneration in zebrafish. *Cell Cycle* 2012;**11**: 1195−201.
30. Deng S, Zhao Q, Zhen L, Zhang C, Liu C, Wang G, et al. Neonatal heart-enriched miR-708 promotes proliferation and stress resistance of cardiomyocytes in rodents. *Theranostics* 2017;**7**:1953−65.
31. Matsuyama D, Kawahara K. Proliferation of neonatal cardiomyocytes by connexin43 knockdown *via* synergistic inactivation of p38 MAPK and increased expression of FGF1. *Basic Res Cardiol* 2009;**104**: 631−42.
32. DiMichele LA, Hakim ZS, Sayers RL, Rojas M, Schwartz RJ, Mack CP, et al. Transient expression of FRNK reveals stage-specific requirement for focal adhesion kinase activity in cardiac growth. *Circ Res* 2009;**104**:1201−8.
33. Li Y, Li Z, Zhang C, Li P, Wu Y, Wang C, et al. Cardiac fibroblast-specific activating transcription factor 3 protects against heart failure by suppressing MAP2K3-p38 signaling. *Circulation* 2017;**135**: 2041−57.
34. González-Terán B, López JA, Rodríguez E, Leiva L, Martínez-Martínez S, Bernal JA, et al. p38γ and δ promote heart hypertrophy by targeting the mTOR-inhibitory protein DEPTOR for degradation. *Nat Commun* 2016;**7**:10477.
35. Zhang B, Zhang P, Tan Y, Feng P, Zhang Z, Liang H, et al. C1q-TNF-related protein-3 attenuates pressure overload-induced cardiac hypertrophy by suppressing the p38/CREB pathway and p38-induced ER stress. *Cell Death Dis* 2019;**10**:520.
36. Yokota T, Li J, Huang J, Xiong Z, Zhang Q, Chan T, et al. p38 Mitogen-activated protein kinase regulates chamber-specific perinatal growth in heart. *J Clin Invest* 2020;**130**:5287−301.
37. Weixler L, Schäringer K, Momoh J, Lüscher B, Feijs KLH, Žaja R. ADP-ribosylation of RNA and DNA: from *in vitro* characterization to *in vivo* function. *Nucleic Acids Res* 2021;**49**:3634−50.
38. Tubbs A, Nussenzweig A. Endogenous DNA damage as a source of genomic instability in cancer. *Cell* 2017;**168**:644−56.

39. Prokhorova E, Agnew T, Wondisford AR, Tellier M, Kaminski N, Beijer D, et al. Unrestrained poly-ADP-ribosylation provides insights into chromatin regulation and human disease. *Mol Cel* 2021;**81**: 2640−55.e8.
40. Challa S, Khulpateea BR, Nandu T, Camacho CV, Ryu KW, Chen H, et al. Ribosome ADP-ribosylation inhibits translation and maintains proteostasis in cancers. *Cell* 2021;**184**:4531−46.e26.
41. Hocsak E, Szabo V, Kalman N, Antus C, Cseh A, Sumegi K, et al. PARP inhibition protects mitochondria and reduces ROS production *via* PARP-1−ATF4−MKP-1−MAPK retrograde pathway. *Free Radic Biol Med* 2017;**108**:770−84.
42. Puente BN, Kimura W, Muralidhar SA, Moon J, Amatruda JF, Phelps KL, et al. The oxygen-rich postnatal environment induces cardiomyocyte cell-cycle arrest through DNA damage response. *Cell* 2014;**157**:565−79.